Two Step Synthesis of ZnO and ZnO@Fe_3S_4 Nanocomposite and its Dielectric Studies

Abid Munir

Reg. No. 00000203264

A dissertation submitted in partial fulfillment of requirements for the Degree of Master of Science in Chemistry

Supervised by

Dr. Azhar Mehmood

Department of Chemistry
School of Natural Sciences
National University of Sciences and Technology
Islamabad, Pakistan

OCTOBER, 2020

FORM TH-4

National University of Sciences & Technology

MS THESIS WORK

We hereby recommend that the dissertation prepared under our supervision by: Abid Munir, Regn No. 00000203264 Titled: Two Step Synthesis of ZnO and ZnO@Fe3S4 Nanocomposite and its Dielectric Studies Be Accepted in partial fulfillment of the requirements for the award of **MS** degree.

Examination Committee Members

1. Name: DR. MANZAR SOHAIL Signature: _____

2. Name: DR. ASAD MUMTAZ Signature: _____

External Examiner: DR. NASIR MEHBOOB Signature: _____

Supervisor's Name DR. AZHAR MAHMOOD Signature: _____

CO-Supervisor's Name DR. HASSAN WAHAB Signature: _____

_____ 02/02/2021
Head of Department Date

COUNTERSINGED

Date: 02-02-2021

_____
Dean/Principal

Declaration

I certify that this research work titled "Two Step Synthesis of ZnO and ZnO@Fe_3S_4 Nanocomposite and its Dielectric Studies*"* is my own work. The work has not been presented elsewhere for assessment. The material that has been used from other sources it has been properly acknowledged / referred.

Signature of Student

ABID MUNIR

2017-NUST-MS-Chem-00000203264

Acknowledgements

All glories to ALLAH Almighty, who persuaded the man with knowledge, intelligence and wisdom. ALLAH's Peace and blessings be upon the Holy Prophet Muhammad (S.A.W), who exhorted his followers to seek knowledge from cradle to grave.

I am greatly thankful to ALLAH almighty for giving me potency, knowledge and opportunity to complete my thesis. Without ALLAH's help and blessings, this accomplishment would not have been possible.

I would like to pay me gratitude to me worthy and scholarly supervisor Dr. ***Azhar Mehmood*** *and Co-Supervisor Dr.* ***Hassan Wahab*** *for their support, guidance and encouragement during my research phase. Under their supervision, I have learned a lot and successfully overcome the difficulties in my research. Their support and courage helped me to complete my research work.*

I am very grateful to my GEC members, Prof. ***Dr. Manzar Sohail*** *and Dr.* ***Dr. Asad Mumtaz*** *for their kind suggestions, encouragement and sparing their valuable time whenever I needed guidance. I am thankful to School of Natural Sciences, NUST for financial support for my project. I am thankful to USPCAS-EN and Pakistan Institute of Nuclear Science and Technology Nilore Islamabad for analysis of my samples. I am thankful to all technical staff.*

Gratitude to my Siblings Ansa Munir, Sana Sadiq, Anila Munir, Kashif Munir and Sadiq Munir, my friends Aatif Niaz, Junaid Ur Rehman, Rana Arslan, Abdul Samad Butt, Zeeshan Asad, and others for their kindness, prayers and moral support during my study.

Abid Munir

Dedicated to my exceptional parents and adored siblings whose tremendous support and cooperation led me to this wonderful accomplishment

Abstract

A novel nanocomposite ZnO@$(Fe_3S_4)_x$ (x=0.6.0.8,1,1.2 and 1.4) was synthesized by using facile two step chemical route. ZnO Nano powder was synthesized through polyol method, using ZnCl2.6H2O as a zinc precursor and other different surfactants NaCl, CTAB (N–Cetyl–N,N,N,trimethyl ammonium bromide) and glycine and ethylene glycol as solvent. Fe_3S_4 nanosheets were synthesized using FeCl3.6H2O and Sulphur (powder) as iron and Sulphur precursor and Ethylenediamine as a solvent. Both products were then transferred to autoclave for 24 hours at kept at 180°C. The product was than filtered washed and calcined at 240°C. The Structural properties of synthesized composite were investigated by X-ray diffraction (XRD), morphology of the samples was examined by scanning electron microscopy (SEM), Fourier transform infra-red microscopy (FTIR) was used to identified the respective bonds while the band gaps and UV absorption were determined by UV-DRS. From XRD we obtain the crystallite size which increases with increasing Fe_3S_4 content but overall, less than pure ZnO. SEM results show that the flower morphology of pure ZnO UV-DRS results shows that with increase with Fe_3S_4 content the band gap of the composite material decreased from 3.35 to 3.06 eV. The dielectric study shows that the dielectric constant of the composite material as compared to the pure ZnO decreases while the dielectric loss in composite material is very low as compared to pure ZnO which has high dielectric loss which means the lower dielectric loss the more effective our composite dielectric material.

List of Tables

List of Figures

TABLE OF CONTENTS

Chapter 1- Introduction

According to the rapid growth of energy generation and storage technologies over the last few decades, the demand for effective energy storing devices and supplying electricity has been substantially increased. Generally, the devices for electrical energy storage can be categorized into two: short-term storage and long-term storage. Each type of device works on different mechanisms and offers a different combination of power density and energy density, as illustrated in Figure 1.1 [1]. In a term of long-term energy storage devices, batteries operate on electrochemical reactions to convert chemical energy into electrical energy and provide high energy density (10-300 W.h/kg) with relatively less power density (less than 500 W/kg). Based on their performance, batteries are suitable for large and stable energy supply applications [2]. On the other hand, capacitors are short-term energy storage devices that use physical charge separation between two electrodes to store energy. Capacitors usually provide low energy density (typically below 30 W.h/kg), but very high-power density (up to 108 W/kg for dielectric capacitors). This means that capacitors can deliver or accept high currents, but only for short periods, due to their comparatively low capacitance. Consequently, capacitors typically apply for electronic and electrical systems that require fast charge-discharge capability or pulsed power applications [3]. Moreover, capacitors can find great potentials in many other fields including power conditioning, signal processing, sensing, and motor starters [4-6]. Although the conventional dielectric capacitors fabricated of dielectric polymers or dielectric ceramics have been widely used in many applications nowadays, it would be still interesting to improve their energy density to be competitive with supercapacitors or even batteries. This may lead to the expansion of their utilization and the reduction of using devices with complex physical structure. The ultimate goal for the research on dielectric capacitors is to achieve the materials with high energy density and high power, low electrical loss, good reliability, compact size, and lightweight.

Communication technologies are developing rapidly, especially mobile communication and wireless communication systems. You can get in touch with your friend by mobile phones, iPad or laptops, which are powerful electronic devices. Microwave resonators and decoupling capacitors are integrated in these systems. To make these functional electronic components, we need high-quality dielectric material with high dielectric quality factor Q ($Q=1/\tan\delta$), low loss tangent($\tan\delta$), large dielectric constant (ε_r), small leakage current, and small temperature coefficient of resonator frequency (for resonators).

1.1. Energy Storing Devices

The rising demand for energy and the use of fossil fuels have a profound effect on environment as well as on the human health. Renewable energy sources have gained a lot of attention and had been used at a faster rate, as a result of which our environment has also shown a rapid decline. To address the issues of energy demand, we need for eco-friendly, highly efficient, and sustainable energy conversion setup and their maintenance. As batteries, and standard capacitors are usually regarded as pure power devices. Depending on the nature of the investment, their performance / capacity may be reduced and the system specified. The power to charge charging of standard capacitors, Super capacitors and batteries is shown in Fig. 1.8. Electric cells and batteries are considered to be a high-power source (~ 105 J Kg^{-1}) but have no power supply (less than 100 W kg^{-1}), while conventional capacitors on the other hand have excellent power supply capacity (106 W Kg^{-1}) but electrical power storage (100 J Kg^{-1}) remains limited[7, 8] .

Batteries and capacitors look the same as they both charge and discharge electrical energy. However, there are important differences between them that affect their applications which may be due to how they work differently.

1.1.1. Batteries

A battery comprises of one or more than one cells which undergo chemical reactions due to which flow of electrons occurs within a circuit. Batteries are needed to store the generated electrical energy so; it can be used when generation is stopped or when power is needed. Here it is noteworthy that only DC can be stored in the batteries while AC current can't be stored.

Battery cells has three main components;

- The Anode
- The Cathode
- The electrolytes

Negative electrode the anode is a that which generate electrons to the external circuit to which the battery is connected. Electrons are accumulated at anode due to which a potential difference is created between the two electrodes. The electrons the naturally try to go back, this process is

prevented by the present electrolyte, so the only way for electrons to travel from anode to cathode is by connecting the battery to external circuit through the electron will flow

Batteries can be categorized into two basic types:

- Primary batteries (Non-rechargeable batteries)
- Secondary batteries (Rechargeable batteries)

1.1.1.1. Non-rechargeable Batteries

Non-rechargeable batteries or primary batteries can be used once. These batteries cannot be recharged so we cannot use it again.

Alkaline batteries

Basic construction of this battery comprises Zinc (Zn) rod at the center of the battery and Manganese dioxide (MnO_2) surrounding it. These two are separated by electrolyte potassium hydroxide which is an alkaline substance that's why battery is named as alkaline battery having.

It has long cycle life, small in size, long shelf life, highly efficient and low leakage. These batteries can be used in torches, wall cloak and small portable electronic gradates.

Figure 1.1 Alkaline batteries

Coin cell batteries

Alkaline composition as also used coil cell batteries. besides from alkaline composition, providing steady and stable voltage in such a small size, lithium and silver oxide chemicals are used which are more efficient. It has Power density of 270 Wh/Kg

Figure 1.2 coin cell

Thy are small and light in weight. They have high density, low cost and long shelf life. They are used in watches and other electronic products etc..

1.1.1.2. Rechargeable Batteries

Rechargeable batteries or secondary batteries can be recharged and can be used again and again. Though the initial cost is high, but the life span is very long when properly used and safely charged.

Common renewable battery chemicals include:

Lead - acid battery

A very cheap lead-acid is used in these batteries and these batteries can be seen mostly in cars and vehicles for powering them. These are more preferable batteries where the size/space and weight doesn't matter. These batteries have a range of voltages from 2V to 24V. The most common of them are 12V batteries. Power density of these batteries are 7 Wh/Kg.

They are cheap and can be charged again for next use.

Figure 1.3 Lead - acid battery

Nickel – cadmium battery (NiCd)

Nickel and Cadmium are the key elements in these batteries. However, these are infrequently used, they are cheap and the discharge rate is low as compared to Ni-MH batteries. The nominal voltage is 1.2V. Power density of these batteries is 60 Wh/Kg.

They are easily recharge come in variety of shapes and size and can be used in all enjoyment.

Figure 1.4 Nickel – cadmium battery

Nickel -metal hydride battery (NiMH)

The Nickel – Metal Hydride batteries are much better choice than Ni-Cad batteries due to its eco-friendly nature. Its nominal voltage is 1.25 V which is slightly greater than Ni-Cad batteries. Its power density is 100 Wh/Kg.

They can be easily recharged they have high power density and they are the better replacement for alkaline batteries

Figure 1.5 Nickel -metal hydride battery

Lithium-ion battery

In these rechargeable batteries' lithium ions migrate towards the positive electrode from the negative electrode during discharging while migrate back from positive electrode toward the negative electrode when the battery is being charged. Due to its compact size, they can be used where high power needed. They are the best rechargeable batteries available till now. These have a nominal voltage of 3.7V and there are number of batteries having different ranges of power capacity (starting from 100s of mAh to 1000s of mAh). Power density of these batteries is 126 Wh/Kg.

Figure 1.6 Lithium-ion battery

They are light in weight and the power density and cell voltage is high.

Lithium-ion polymer battery

Due to use of highly conductivity polymer electrolyte in it these are called as Lithium Ion polymer batteries. They can categorize in Li-ion technology. These are a costly. As compared to the Li-ion batteries these batteries are very highly protected. These batteries have Power density of 185 Wh/Kg.

Figure 1.7 Lithium-ion polymer battery

they are light in weight very thon in structure wise and the nominal voltage and power density is slightly higher than Li-ion batteries.

1.1.2. Capacitors

Capacitors are widely used in electronics for storing energy. Capacitors can charge and discharge electricity very quickly. It is also used to block the flow of DC. This function is implemented where specific frequency is required. Capacitors can store little amounts of energy compared to batteries but can discharge the energy very quickly, meaning they have high power density. Pulsed power electronics needs quick power for short time that can be delivered only by capacitors. In order to scale down electronics devices development of capacitors that has high energy density and high-volume efficiency is required[9] .

The reason capacitors can charge and discharge quicker than batteries is that electrochemical reaction takes place in batteries where static charge is stored in capacitors. High performance lithium ion battery has limitations like low power density and low durability but capacitor can perform much longer than battery. **Figure 1.8** shows energy and power densities of capacitors and batteries. Capacitors have highest specific power than any other energy storage devices.

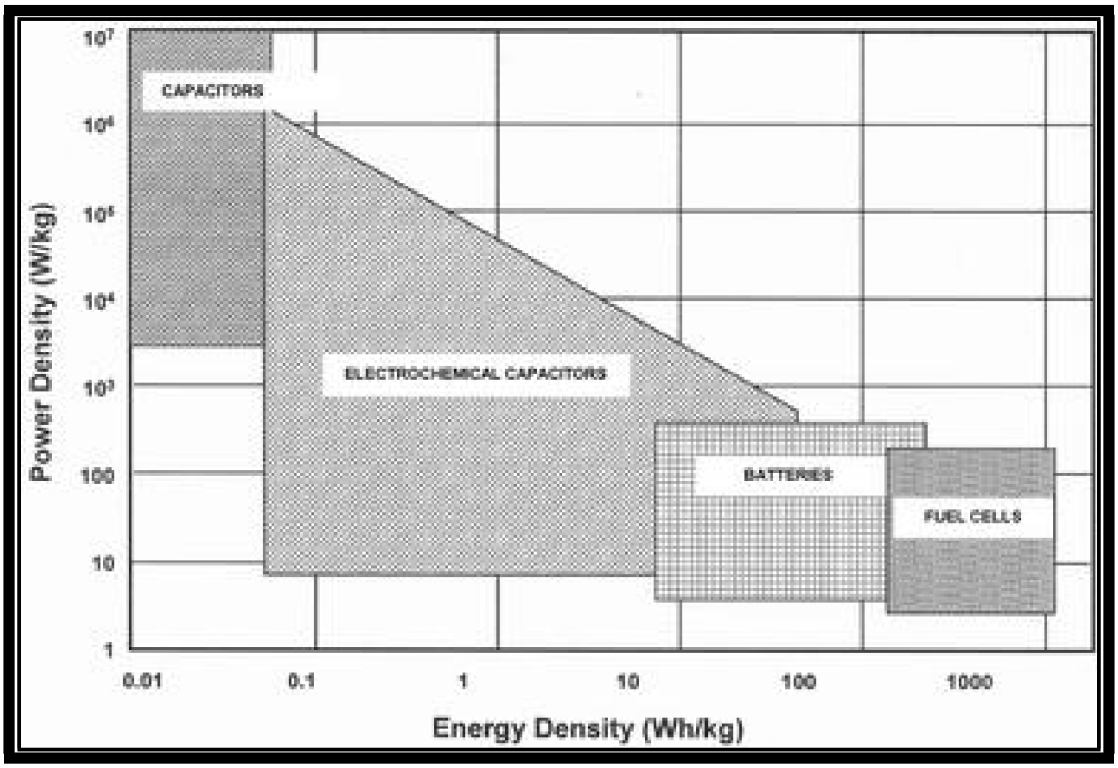

Figure 1.8 Simplified Ragone plot of the various energy storage devices [10]

There are basically three type of Capacitors:

1.1.2.1. Dielectric Capacitor:

Dielectric capacitors are usually a flexible type where nonstop power variation is required for the transmission, transmission and radio transmissions of the transistor.

Variable Capacitor Symbol

Various dielectric capacitors are types of air-separated plates with stainless steel plates and a set of moving plates moving between two fixed plates. Total capacitance value is determined by the position of the moving plates in relation to the fixed plates. The capacitance is usually at a high level when the two sets of plates are fully integrated. High power repair capacitors have large spaces or air spaces between plates with breaking values up to several thousand volts.

1.1.2.2. Electrolytic Capacitor*:*

Electrolytic capacitors are the most widely used capacitors with tolerant potential. These are available with active volumes up to 500V, although very high capacitance values are not available at high voltages and high temperature. There are two types of electrolytic capacitor, tantalum and aluminum.

1.1.2.3. Super capacitor (SC):

Super capacitors contain a family of electrochemical capacitors. Super capacitor, sometimes called ultracapacitor is the common name for double-layer electric capacitors (EDLC), pseudo-capacitors and hybrid capacitors. They do not have a conventional dielectric. Electrochemical capacitors capacitance is determined by two parameters, both of these contribute to the capacitor capacitance:

Double-layer capacitance

Pseudo-capacitance

1.1.3. Dielectric Capacitor:

Typically, a dielectric capacitor has two parallel plates running area A which is separated by certain dielectric elements by size d, as shown in Figure **1.3** [1]. Theoretically, the external voltage energy applied to conductors can cause electrical polarization in dielectric objects. To compensate for this

polarization, positive and negative charges with equal amount are accumulated on two plates, respectively, called a capacitor charging process. The process will be completed when the electrical energy generated by the values collected Q in both plates equal to the external energy used V. The energy storage capacity of a capacitor, called capacitance C, can be defined as

$$C=Q/V$$

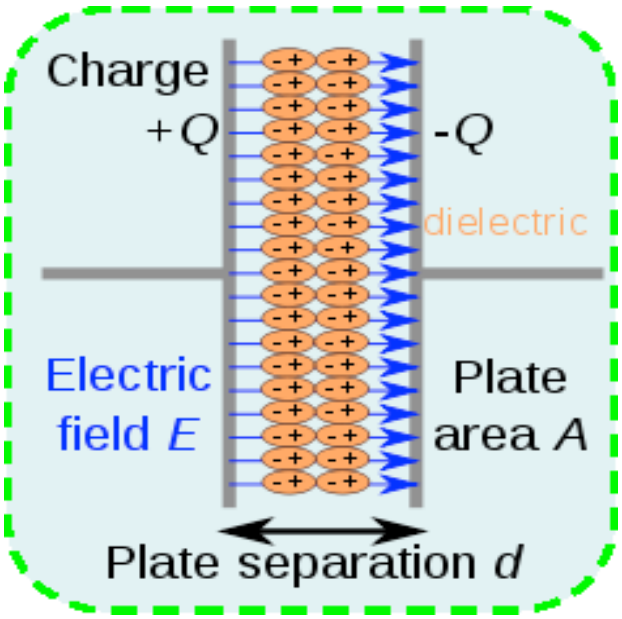

Figure 1.9 Charge separation in a capacitor under external electric field.

In addition, the capacitance of a parallel capacitor plate can be determined as a function of its body size and dielectric clearance, as described in the following equation:

$$C = \varepsilon_r \varepsilon_0 A / d$$

where C is capacitance, the surface area of the plate is denoted by A, while the distance between the two parallel plates is denoted by d, r the relative permittivity of the dielectric material, and ε_0 is the permittivity in vacuum (8.85×10^{-12} F / m). Depending on the equation, the capacitance is directly proportional to the relative dielectric permittivity and the surface area of the plates, while being proportional to the size of the particle. It is clear that the power of the capacitor does not depend on both the potential difference between the operating plates and the total values charged on them.

1.1.4. Dielectric Theory

A clear guide to dielectric theory is provided by Kao.[11] . A dielectric is basically insulator material (electrically) which polarizes by applying external electric field. In term of DC (direct current) insulator is an object with low conductivity (electrical). While in AC terminology the word dielectric is used exclusively, referring to a material which can be polarized easily. One of the most important properties of a dielectric material is the relative permittivity, also called dielectric constant. Dielectric constant of an object is a measure of the polarizability of an object with the use of an alternating electric field. The classification of an object depends largely on the chemical composition and imperfection (defects) of the object and on other parameters including pressure, temperature and processing conditions.

Atoms or molecules in dielectric materials polarizes through five basic types:

• Electronic polarization

• Atomic or ionic polarization

• Orientational polarization

• Interface or space charge polarization

At different scale time specific polarization occurs; that is why the time variation of the electric field has huge impact on the overall degree of polarization. The amount of time depends largely on the size of the polarized species. **Figure 1.10** shows the different polarization at different frequency.

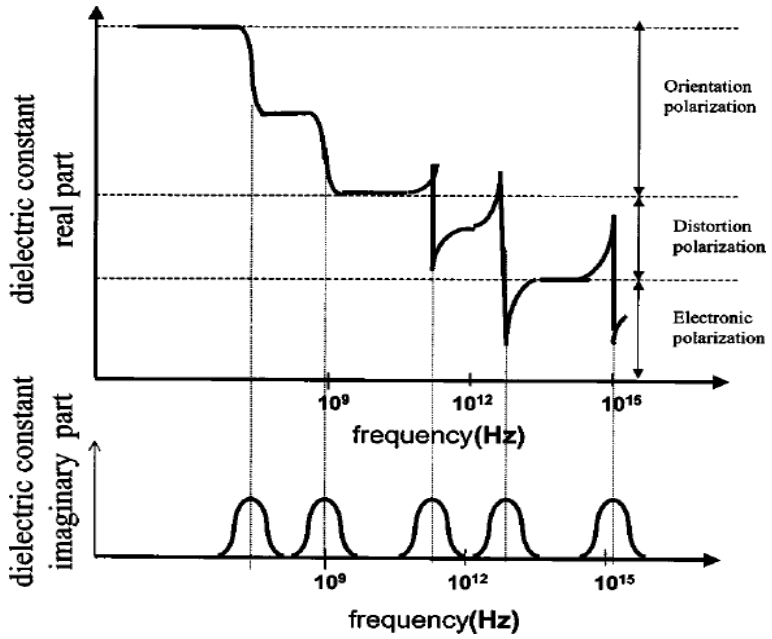

Figure 1.10 polarization mechanisms vs function of frequency[12]

Polarization occurs instantly when the relaxation time is faster than the frequency of the external electric field. And there is no polarization when the relaxation time is slower than the frequency of the external electric field. Energy is absorbed by the dielectric material when the relaxation time and the frequency of the external electric field is same. This is called dielectric Loss. It is measured by the relationship $\tan\delta = \varepsilon'_r / \varepsilon'_r$ where ε''_r is always considered the dielectric imaginary part and ε'_r is the real part of the dielectric variable.

There are three major mechanisms for electronic polarization into moderate electrical fields (i.e. in the lower extremities than the internal atomic or molecular field) and where objects have very low conductivity (i.e. the concentration of internal charge carriers is so low that if the results can be small). These are:

• ***Electronic polarization***: By applying external electric field the original symmetrical distribution gets distorted or translated of electron atoms or molecules. This is actually the migration of outer electron clouds in relation to the positive internal atomic nucleus.

• ***Atomic or ionic polarization***: Displacement of atoms or ions with respect to each other occurs by applying external electric field. This is actually a distortion of the normal lattice vibration.

• ***Orientational polarization***: Material containing molecules have this type polarization. The electric field causes the reorganization of the dipoles in the direction of the field.

Electronic and atomic polarization are mainly caused by the elastic migration of electron clouds and the vibration of the lattice within the atom or molecules. The polarization process of electronic and atomic polarization is slightly dependent to temperature because of the insensitivity to the temperature of the restoring force against displacement. Orientation polarization is only observed in molecules and it is also called rotational process. Under the application of external force, it attains equilibrium state. When field is removed, it returns back to its original state.

In ‘’lossy” materials and in high fields the injection of carrier is essential. In a concentrated charge carrier material, the polarization at interfaces and grain boundaries create space charges due to migration of charge carriers. This type of polarization is called **space charge polarization.**

The total polarizability of a materials, α, is a sum of all polarization processes $\alpha = \alpha e + \alpha i + \alpha o + \alpha$

where $\alpha_e + \alpha_i + \alpha_o + \alpha_d$ is a component of electron, atomic, orientational, and -space charge, respectively.

Chapter 2- Literature Review

The production and use of energy depend on improving the quality of our lives. Major economic developments in recent decades have led to increased demand for energy, which is largely provided by renewable resources such as natural gas, oil, and coal[13, 14] . Some serious concerns have been caused by these traditional energy sources by strongly relying on them. The unequal distribution of resources and the uninterrupted supply of mineral oil, results environmental problems such as atmospheric pollution and global warming.[15, 16] . In this regard, new technologies on a large scale are needed that are capable of transforming and conserving energy for the sustainable development of our economy and society[17, 18] . Environmentally friendly and renewable energy production has been improved and improved over the years, which has led to extensive and varied research in the scientific field of material sciences. Active nanomaterials with potential for converting energy and devices for storing energy, such as solar cells, fuel cells, capacitors, supercapacitors and renewable batteries, are widely studied[19-21] . Power generation and catalysis sciences are the taking advantage of the energy provided by the nanomaterials not only by a well-established catalyst of nanoparticles but also by new solar films, green coverings, highly efficient fuel, and sensing [22].

In the case of nanomaterials, the size and shape of its particle plays a great influence on material properties. In nanotechnology a particle acts as an entire unit in terms of its properties. According to size coarse particles have diameter between 10,000 and 2,500 nm. Fine particles having range between of 2,500 to 100nm. Nanoparticles or ultrafine particles are sized between 100 and 1 nm. A bulk material must have persistent physical properties irrespective of its size and size dependent properties are frequently perceived at the Nano regime. Consequently, the properties of materials change as their size reaches the nanoscale where quantum confinement phenomenon is witnessed and the number of atoms at the material surface becomes important and significant. Due to large ratio surface area to volume, the exciting properties of nanoparticles are observed as the number of atoms at the materials surface is in relation to the number of atoms in the bulk material [23] the number of atoms at surface and at the interface increases with the decrease in size of and dimension of the particle and strongly influencing the reactivity of material with respect to bulk material in the oxide nanoparticle. Another important property of the oxides is electronic property which is greatly affected by size of the particle. In nanomaterials the electronic configuration is also

different from that of the bulk materials. By reducing the particle size, the magnitude of the energy levels also changes which leads to a significant change in the material's optical and electrical properties[24] . Therefore, the nanoscale formation can effectively improve the efficiency of an electrochemical reaction. Nanomaterials became a major focus of research, aimed at refining the surface morphology of bulk materials, harmonizing and assembling functional properties to produce the most efficient and powerful next generation power devices. of strength and power to increase their performance.

Due to unique properties such as low molecular weight, low toxicity, good electrochemical properties and solid properties [25-28] metal oxides have gained a lot of attraction among many nanomaterials which is used for energy consumption. The unique properties of these metal oxides are particularly important in many areas and with various uses, such as catalysis, sensors, absorbents, ceramics and superconductors (Fig. 2.1)[29-34] . Metal elements have ability to form diverse class of metal oxides, and can accommodate different structural geometries that may reflect metal, semiconductor, or insulator character[35] .

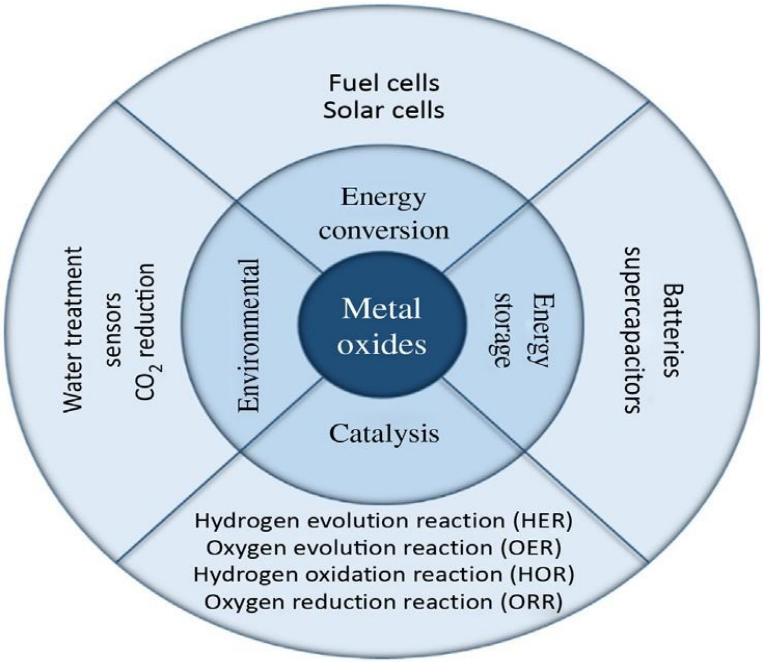

Figure 2.1 Application of metal oxides.

Metal oxides attract special attention because of their simple formation mechanism and active behavior and therefore they are studied exclusively for generating energy and energy storage

systems, mainly due to the potential for high-performance electrode surface, resulting in high charge/discharge rates, and their rich redox response involving different ions[36] (Fig **2.1**).

2.1. ZINC OXIDE MATERIAL PROPERTIES

The unique and interesting features of the combined II-VI semiconductors have created great incentives for scientists to explore the potential for use in industrial systems An "n'' type semiconductor Zinc oxide has optical, electrical, optoelectrical, piezoelectrical, and many other important applications due to its wide band gap (3.37 eV) at 25^{o}C and high electron hole binding energy (60 meV)[38, 39]. Wurtzite is the most stable form of zinc oxide which lacking center of symmetry and has large electrochemical coupling. Zinc oxide has piezoelectric, pyroelectric properties, emits light of short wavelength and appropriate doping makes it electrically conductive. Zinc oxide is also nontoxic, biocompatible and biodegradable which extends the area of its biological application [37]. Discovery of zinc oxide nanobelt in 2001 has created research interest in zinc oxide nanostructure[38] . Intensive research has been done on zinc oxide nanostructures because of their ease of synthesis process and better electrochemical properties. Electron diffusion rate can be heavily increased by increasing surface area of nanostructures. Zinc oxide has electron mobility of 200 cm2 V^{-1} at room temperature in single crystal form. Zinc oxide offers better resistance to radiation than gallium nitride which makes it more desirable for nuclear plant and space use.

As a Piezoelectric transducer, as a catalyst and a photonic material ZnO is widely used. Over its main competitors GaN and SiC, ZnO has some basic advantages. That is due to its high binding energy to 60 meV, which is much higher than that of GaN (21-25 meV); the strength of high-energy radiation and the intensity of water-based chemistry (although both are better than Si or GaAs) In addition, many experiments have confirmed that ZnO is highly resistant to high-intensity radiation, making it applicable to be used in space. In acids and alkalis, it can be easily absorbed. Due to this, it can be used in the manufacturing of small electronic devices e.g. solar cells, transparent electrodes and display window items. It also contains a native substrate[39] . In addition, the technical applications of ZnO, includes porcelain

enamel, heat-resistant glass, rubber and plastic additives, activator in vulcanization, pigment paint with UV and fungistatic properties, protective spacecraft, tobacco filtering area, therapeutic ointments, wavelengths, and much more [40].In the development of transducers of small transparent film (TFT), ZnO has played a vital role, by placing a layer on a flexible substrate at low temperature , detecting transparent TFTs, and performing additional functions such as photodetections using the ZnO channel. In this case the protecting cover to stop light exposure is removed because ZnO transistors are not sensitive to visible light[41, 42].

Cadmium oxide (CdO), indium tin oxide (ITO) and Zinc oxide (ZnO) films have been studied in recent years as Transparent conductive *oxides (TCO)* due to their exceptional electrical and light properties combined with a large belt gap (> 3ev), environmental degradation, visual acuity (> 80%) in the visual region and non-toxicity[40].

In past decade, due to high electrical permittivity ZnO nanoparticles have been considered as a conductive filler in polymers and they have also gained attention for their potential application in high charge-storage capacitors [8]. Dangling bonds, micropores, and vacancies are the defects in ZnO structures, which are present in grain boundaries or at the interfaces that can play a vital role in their transport properties. Impedance spectroscopy can easily determine the role of grain and grain boundaries [9, 10]. However, there are few reports on the dielectric behavior and transport properties of ZnO have been reported and with composite of ZnO with Transition metal dichalcogenides (TMD) are none. In nanometer range the high surface-to-volume ratio of ZnO will significantly change their electrical properties as compared to those of the bulk material and these properties will be more interesting when composite is formed with TMDs. Thus, the study of overall dielectric performance and electrical transport of this composite material is very important.

2.1.1. Fundamental properties of ZnO

2.1.1.1. Crystal structure

Zinc oxide exists in three form of crystal: stable and abundant (hexagonal), zinc blende (cubic), and r rock salt (cubic) which is rare as to compared to other two forms. The stability of wurtzite structure greater than the others therefore it is very common in the normal conditions. Zincblende can be easily grown on substrates having cubic lattice structure. The possibility of NaCl-type rock salt can be seen only at very high pressures ~10GPa. The inversion symmetry of hexagonal wurtzite and zincblende is not possible (crystal reflection compared to any given point does not convert itself). Lattice constant is = 3.25 Å and c = 5.2 Å; the ratio of c to a is c / a ~ 1.60 which is close to standard value of the cell c / a = 1.633. in most of the II-VI materials, the strong piezoelectricity of ZnO is explained by large ionic bonding in ZnO. Due to this ionic character, planes of zinc and oxygen carries electric charge.

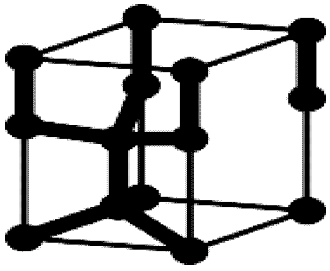

Figure 2.2: wurtzite ZnO structure.

2.1.1.2. Electronic band structure

A prominent character of any given semi-conductor is its band gap, as its activity is related to the energy difference of the conduction band and valence bands along with the number of active electrons and holes present. Among its family, ZnO is considered to be the best candidate for its abundance, easy heating at normal condition under UV filament and more opportunities to create different band gaps by doping it with other materials so that the constructed electrical structures can work best under all conditions.

Normally methods that are used to determine band formation include performance under UV, morphological changes observed either by XRF or XPS, were employed to determine the positions of lattice parameters. The difference of energy between different electronic levels (for example, transitions from the upper valence-band states to the upper conduction states, and the lower valence-band states) are basically measured by these methods.[39, 40, 43].

The most important feature of the ZnO band structure is that it has a band gap. Tight-binding Hamiltonian operation was employed to determine band structures and result revealed a direct band gap, with a value of 3.3 eV and is actually the energy difference between empty and filled states.

If you look at the figure, the lower position is termed as valence band and the upper border of this region is called valence band edge while the empty positions on the top is known as conduction band and its lower border is called conduction band edge. For ZnO both the conduction band edge and valence band edge are located at same energy also called zero energy, so the material is called direct band gap material[44, 45].

2.1.1.3. Optical Properties

Properties found to be associated with optical activity were reckon by intrinsic and extrinsic character. It is observed that when group velocities of electron in conduction band and holes in valence band are equal, results in excitation formation under the influence of Coulombic interaction lead to intrinsic optical transitions. Excitations are grouped as either free excitons or bound excitons. In pure sample where there are less chances of the presence of foreign species, free excitons also undergo excited transitions along with Ground state conditions.

Extrinsic properties come into play when there is a dopant or a defect is created under special conditions, which results in the formation of discrete electronic states, thus govern variation in optical absorption and emissions. As discussed earlier, ZnO also known as direct band semi-conductor is transparent conductive crystal. Its thin films appear transparent under light's wavelength ranging 0.3μm-2.5μm. It is also observed that a shift in band gap appear when the concentration of carrier, called Burstein-Moss shift. Different spectroscopic techniques were employed to study optical transitions in ZnO.

When PL spectrum of ZnO is obtained at room temperature, showed near UV band at 375nm along with green emission band at 510nm while orange-yellow band at 610nm is also observed in some cases. Studies revealed that near UV band appeared due to excited behavior of material which is supposed by free exciton release, so it is called bound exciton emission or bi-exciton emission. Even at low temperatures it is sometimes became very difficult to observe luminescence. This happens due to certain reasons including[46]

- The radiative emission's productivity is quite low even for semi-conductors with direct band gap. A prominent portion of radiative emission arise due to defect centers in crystals and bound exciton processes.
- The exciton emission is limited due to internal reflection of exciton along with small escape length. Its serves as a quasi-particle and moves through semi-conductor with their group velocity.

During the motion of electron there are chances of scattering or hindrance by impurities, but when it reaches the surface total internal reflection takes place and is bounced back into the material. Beside internal reflection, the radiative emission apart from free exciton is also restricted by small escape length, only the free exciton present within escape length contribute towards luminescence.

As discussed earlier a green band at 510nm is also a great dimension for researchers, began in the early stages of the last century. Because of this emission, ZnO is known as important luminescence material especially used in planar display and short decay cathode-luminescence screens, but mechanism behind it is still doubtful.

2.1.1.4. Electrical Properties

As ZnO is a direct band gap semi-conductor having large excitation binding energy, is a strong candidate for opto-electronic and electronic devices. For instance, a device made of material having a larger band gap will have higher break down voltage, will generate lesser noise and operates at higher temperatures with prominent output. Th electron transport chain inside semi-conductor will behave differently at different strengths of electric field. At lower

strength of electric field, the electron transport chain is very little or remain unaffected, as the electron can't get much acceleration from the applied electric field as compared to their thermal energy. So, the movement of electrons will remain constant as the scattering rate which determines it remains same.

When the strength of electric field increases, the energy gained by electron will become equal to their thermal energy, so their distribution functions deviates from equilibrium status. As a result, electron temperature increases but not so much that the lattice is destroyed and no loss was observed during this short critical time. Devices with higher frequencies can be fabricated when the electron's drifting velocity became higher than its steady state velocity.

2.1.1.5. ZINC OXIDE PIEZOELECTRIC EFFECT

Many wireless electrical devices require less power and power will keep them stable. Zinc oxide nanowires and titanate nanowires can be used to harvest energy due to their pie properties. All electronic components have the same way of generating electricity from a type of machine. Here the piezoelectric effect of zinc oxide is described. Zinc oxide has a non-centrosymmetric structure in which oxygen and zinc atoms are synthesized tetrahedrally. Any external mechanical pressure can cause lattice disruption leading to the removal of positive and negative charges[47]. Local dipole moment is formed and as a result the moment of macroscopic dipole emerges throughout the crystal. Zinc oxide provides the highest pie properties among other tetrahedrally bound semiconductors[48].

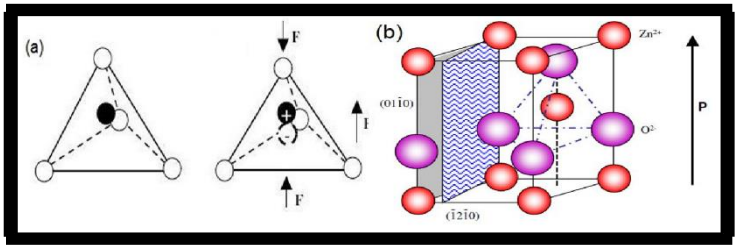

Figure 2.3: (a) piezoelectric effect in a tetrahedrally ZnO unit cell [48]. (b) The wurtzite model of ZnO[49].

ZnO is an important semiconductor (Eg = 3.37 eV) of the II-VI group, which has many applications for gas sensors, lasers, field extraction, solar cells, and photodetectors[50-55]. However, despite

its high potency, certain problems always affect the performance of ZnO nanomaterials, including chemical instability as opposed to response solutions and internal defects that still prevent their integration into product use[56]. Surface coating (or surface modification) has been seen as one of the most advanced and interesting ways to create compatible nanomaterials[57], as a result of introducing something else to ZnO to expand its application space into a viable medium. For example[58] also designed and modified ZnO nanowire (NW) / CdS film heterostructure for hydrothermal growth. The results showed that the heterostructure was optimized as it had significant improvements in the performance of imaging structures and the device would play an important role in the field of UV acquisition[59] we have combined the TiO2-ZnO circular composite series in a simple twostep form, its absorption band that exhibits a specific reddish transformation and all have a higher photocatalytic function compared to pure ZnO.[60] ZnOCdSe building sheets have been developed in a simple way to aid growth. ZnO-CdSe sheets of hetero-structural sheet showed a progressive level of hydrogen photocatalytic under more visible light than ZnO sheets, CdSe NPs. However, to our knowledge, there are no reports of ZnO / Fe_3S_4 composite formulation and their use in dielectrics. In this paper, we present a step-by-step chemical route preparation for ZnO/ Fe_3S_4 nanocomposites. The samples were characterized by using a number of techniques, and it was found that the resulting mixture was composed of hexagonal ZnO nanoflowers and cubic Fe_3S_4 nanosheets, while Fe_3S_4 nanosheets grown on the outer part of the ZnO. The prepared samples were then characterized by various experimental techniques.

Chapter 3-Experimental work and Characterization techniques

3.1. Experimental work

3.1.1. Synthesis of ZnO

Zinc Oxide was synthesized by using Polyol method [61].

Materials

S.No	Chemical	Manufacturer	Purity
1	Zinc Chloride Hexahydrate	Sigma	98%
2	Glycine	Merck	99%
3	Cetyl trimethylammonium bromide (CTAB)	Dae Jung	99%
4	Sodium Chloride	Sigma	99%
5	Ethylene Glycol	Merck	99.8%
6	Sodium hydroxide	Merck	97%

Table:1 Chemicals used for Zinc Oxide synthesis

Procedure

20 mmol of ZnCl2.6H2O, 5.2 grams of NaCl, 10 grams of Glycine and 10 grams of Cetyl trimethylammonium bromide (CTAB) were dissolved in 200 ml of ethylene glycol. The mixture was then heated at 200°C under continues stirring. At first the solution was turned milky, after 15 minute the solution turned yellow and finally it becomes dark brown. At this stage the heating was stopped and solution was further stirred for 30 minutes. After that the dark brown solution was poured into pre-prepared 1M NaOH solution and left overnight for the precipitation of ZnO nanoparticles. Next day the precipitates were collected washed with ethanol and water 5 times and then finally dried.

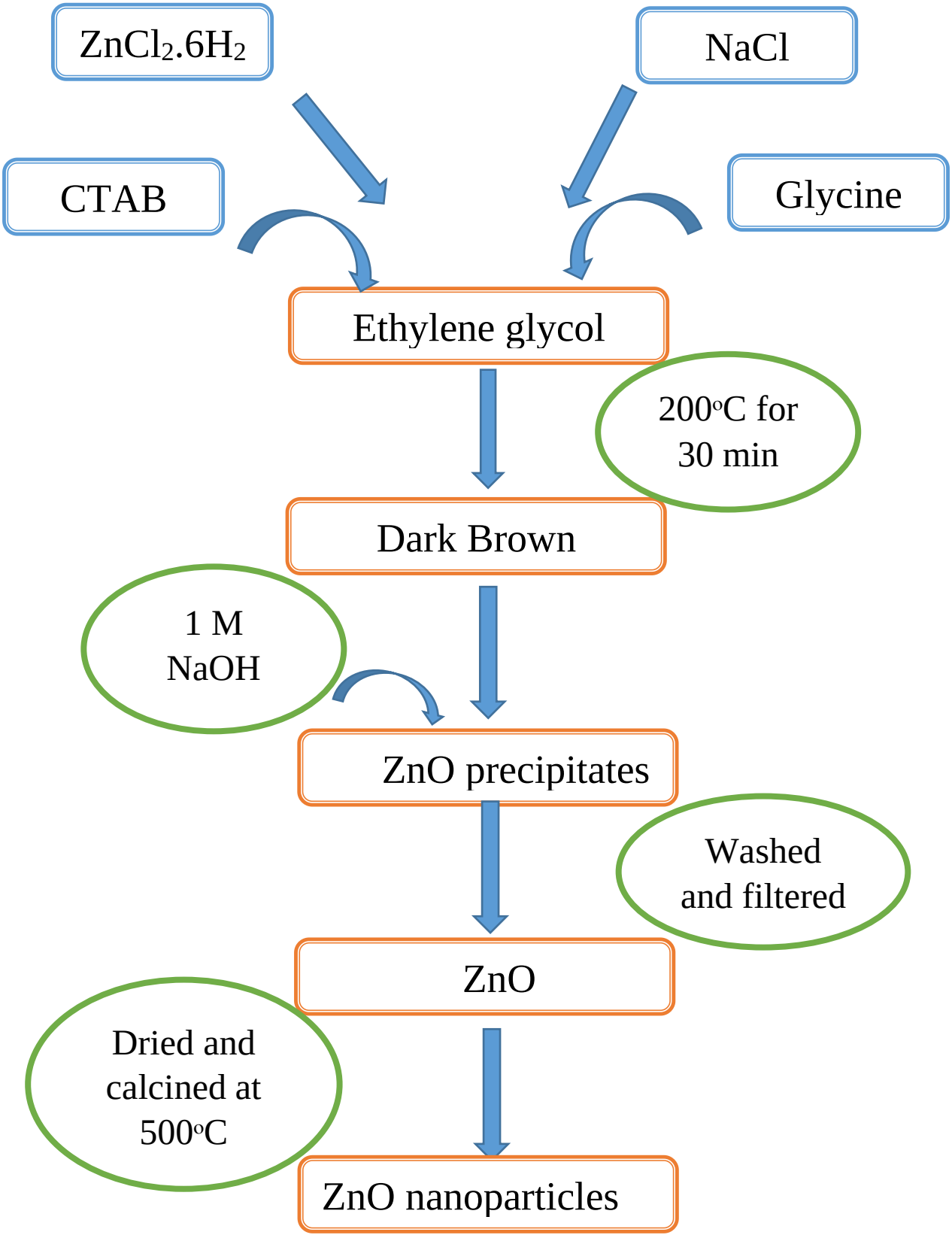

Figure 3.1: schematic representation of ZnO nanoparticle

3.1.2. Synthesis of ZnO@ Fe_3S_4

S No	Chemical	Manufacturer	Purity
1	$FeCl_3.6H_2O$	Merck	98%
2	Sulphur	Honeywell	99%
3	Ethylene diamine	Merck	98%

Table 2: Chemicals used for ZnO@ Fe_3S_4 synthesis

Firstly, the as prepared ZnO nanoparticles and CTAB were dispersed ultrasonically in 20 ml ethanol until it becomes homogenous solution. The solution was marked A. In second step the synthesis of Fe_3S_4 Nano sheets was carried out in three-neck flask. Where $FeCl_3.6H_2O$ was dissolved in ethylene diamine under magnetic stirring and the temperature was gradually increased to 140°C and kept at 140°C until it is completely dissolved and gives yellowish transparent solution. Also, Argon gas was purged to the flask for providing inert atmosphere. In parallel Sulphur was also dissolved in separate beaker in ethylene diamine at 140°C. The dissolved Sulphur solution was then injected into $FeCl_3.6H_2O$ solution through one of the necks. After that the temperature was gradually increased to 240°C and the color of the solution changes from brown to greenish. At this stage the heating was stopped and left for 30 minutes under stirring. After 30 minutes stirring was stopped and the solution was marked B. Both the solution A and B were then mixed and transferred into 150 ml Teflon liner autoclave and was then sealed tight and kept for 24 hours at 180°C. The autoclave was air cooled to room temperature. The precipitates were then washed with ethanol and hexane from impurities and finally vacuum dried and calcined at 240°C for 6 hours. By this method we synthesized five different sample which are listed in the table 3.

Sr No	Sample ID ZnO@ $(Fe_3S_4)_x$	ZnO (grams)	$FeCl_3.6H_2O$ (grams)	Sulphur (grams)	Ethylene diamine(ml)
1	ZnO@ $(Fe_3S_4)_{0.6}$	1 g	1.848 g	0.21 g	10 ml
2	ZnO@ $(Fe_3S_4)_{0.8}$	1 g	2.463 g	0.29 g	20 ml
3	ZnO@ $(Fe_3S_4)_1$	1 g	3.071 g	0.36 g	30 ml
4	ZnO@ $(Fe_3S_4)_{1.2}$	1 g	3.967 g	0.43 g	40 ml
5	ZnO@ $(Fe_3S_4)_{1.4}$	1 g	4.311 g	0.5 g	50 ml

Table 3: different ratios of ZnO@ Fe_3S_4

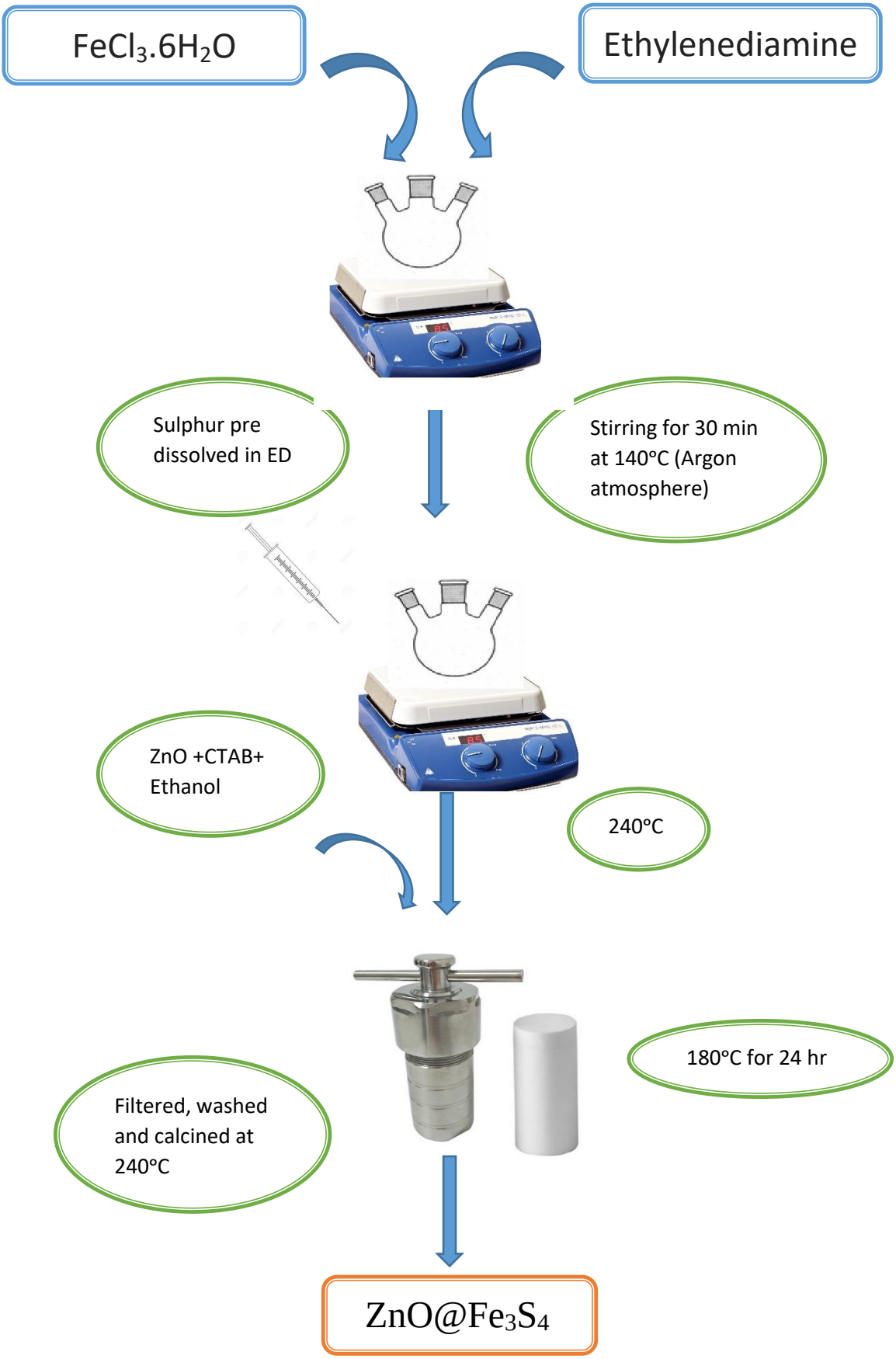

Figure 3.2: schematic representation of ZnO@Fe_3S_4 nanoparticle

3.2. Characterization Techniques

Characterization and analytical techniques are used to analyze materials. These techniques give information about physical as well as chemical properties. They include spectroscopy, chromatography gravimetric and electrochemical analysis etc. In -this work I have used number of analytical methods for confirmation of prepared samples and to analyze their electrochemical properties.

3.2.1. X-Ray Diffraction (XRD)

X-ray diffraction is a distinctive nondestructive technique to determine the crystallinity of synthesized materials. XRD analysis is only used for samples in crystalline forms. According to A. W. Hull (1919) "all the crystalline materials offer arrangements; similar substances always offer similar pattern and in the mixture each element provide its particular configuration independent of other". Therefore, it is used as a finger- printing apparatus to classify the crystal configuration, numerous polymorphic arrangements, ideal crystal alignment, percent crystallinity and additional parameters like average grain size, crystal imperfections and strain. XRD leads to classify components of sample and area under peak provides comparative amount of each element present.

Bragg examined the diffraction phenomenon of x-rays from crystal planes. When x-rays strike the two neighboring layers of solid crystal are scattered. The reflected beam of lower plane of crystal travels extra distance as compared to the beam by upper plane of crystal. Constructive interference of these monochromatic x-rays diffracted from lattice planes at definite angles give peaks and constructive interference is merely possible when Bragg's law ($\boldsymbol{n\lambda=2dsin}\ \Theta$) is satisfied[62, 63] . Bragg's diffraction is schematically illustrated in **Fig. 3.1**. It describes the interference configuration of x-rays scattered by crystal and offers relation among wavelength of electromagnetic radiations, diffraction angle and lattice spacing. The results from XRD investigations are achieved in the system of diffractogram, which is a plot of intensity verses diffraction angle.

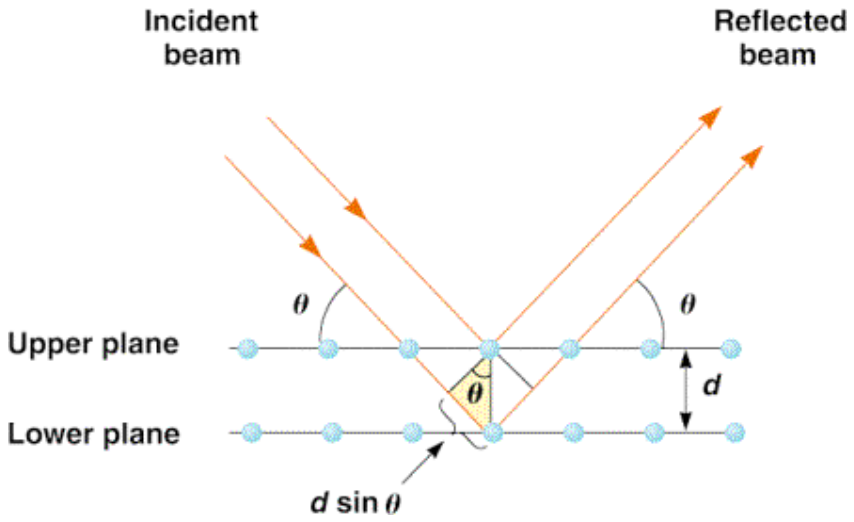

Figure 3.3: Schematic illustration of Bragg's diffraction

X-ray diffractometer consists of three main components: x-ray tube, sample holder and x-ray detector as shown in **Fig. 3.4**

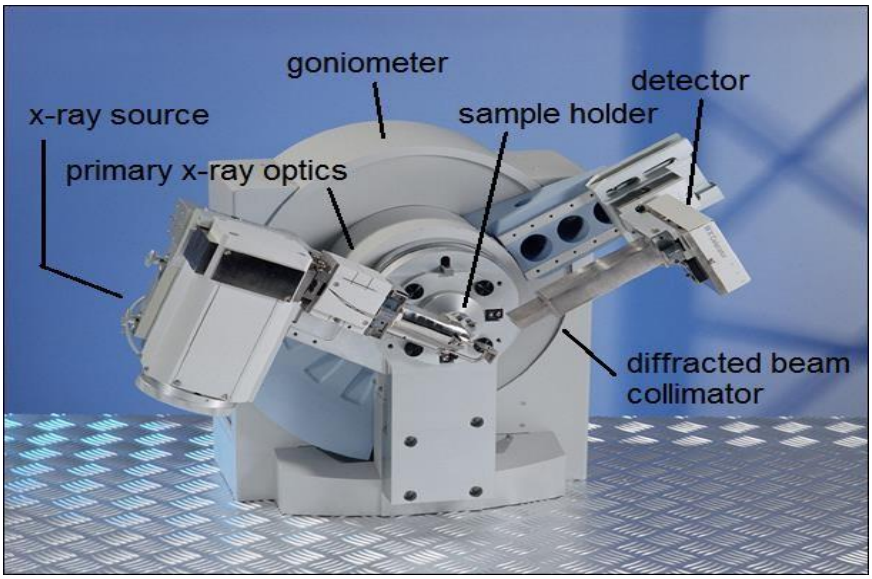

Figure 3.4: main components of X- ray powder diffractometer

Ray tube also named as cathode ray tube comprises of negatively charged metal cathode and positively charged target anode such as Cu, Fe, Cr, Mo or Rh. In the cathode ray tube electrons are produced by heated filament that is blasted on metal anode to produce x- rays. Only electrons having enough energy to disrupt inner shell electrons are capable of generating x-rays. These x-rays are filtered over monochromator, collimated and focused on the sample. **Fig. 3.5** is schematic representation of path followed by x-ray beam after passing through sample. The X-ray diffractometers is built in a manner that rotation of sample at an angle θ is carried out in x-rays path. The instrument used for the rotation of sample and detector is named "goniometer". X-ray detector switches at an angle of 2θ and is static on a support medium for the collection of diffracted x-rays. Constructive interference of incident beam of x-rays with crystal-like sample provides XRD configuration when passing over the detector [63, 64].

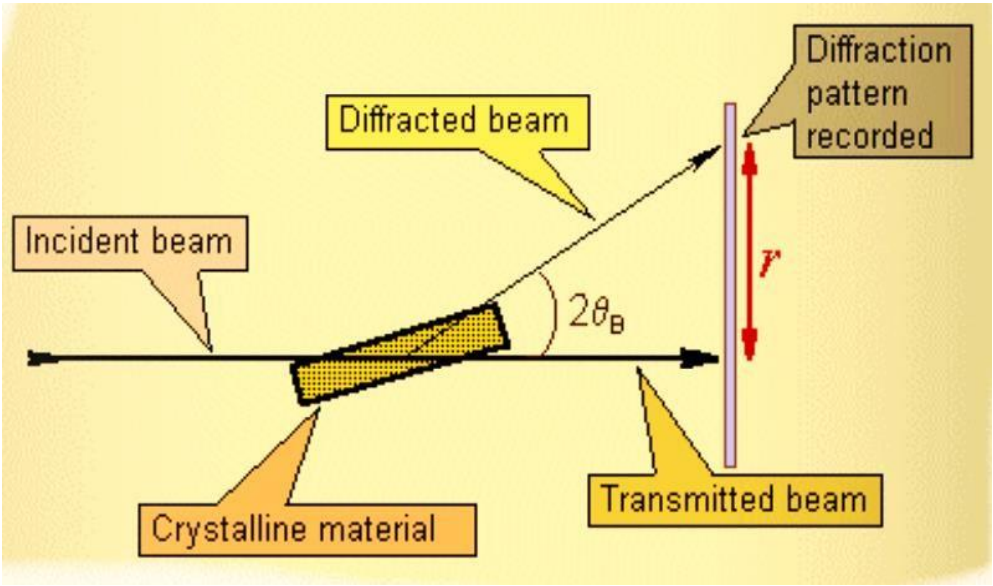

Figure 3.5: path followed by X-ray beam after striking sample X-ray diffraction

- Classify unknown crystalline material, phases and orientation
- Identify fine minerals like kaolinite
- Determination of sample purity
- Identification of unit cell dimensions
- To analyze thin films thickness
- Determination of structural properties such as strain, grain size, , epitaxy, thermal expansion and phase composition

3.2.2. Fourier Transform Infrared Spectroscopy (FT-IR)

Fourier transform infrared spectroscopy (FTIR) is promising analytical technique used to determine bonds in compounds and functional groups present in molecules or on the surface of synthesized materials. The wavelength range of infrared region is 4000 cm^{-1} to 400 cm^{-1}. Vibrations of atoms can be measured by using IR spectroscopy, which helps in determining functional groups [65].

Basic principle of FT-IR involves the excitation of molecules from lower vibrational energy state to higher vibrational energy state i-e from ground state to excited state, when infrared radiations pass through them. In FT-IR, spectroscopy only those frequencies are absorbed which match with the vibrational frequency of bond therefore it is also known as vibrational spectroscopy. The distance between nuclei of atoms in molecules, increases as a result of absorption of IR radiation while the frequency of vibration does not change so each molecule requires quantized energy to promote it to higher vibrational energy level [66]. IR spectrum is mostly represented as a plot of absorbance versus wavenumber.

FT-IR spectrophotometer consists of source of radiation, sample compartment, optical chopper, monochromator, detector, amplifier and recorder as shown in **Fig. 3.6.** Sources of radiation are Nernst filament and Globar filament. Nernst filament is composed of oxides of zirconium, thorium and yttrium and is in the form of hollow cylinder of 2 mm in diameter and 20 mm in length whereas Globar is a bonded silicon carbide rod of 5-7 mm diameter and 50 mm length. When these rods are electrically heated from 1500-2200 K, they emit infrared radiations. The radiation produced by source is divided into two beams of equal intensity. One beam passes through the sample while the other acts as a reference beam. The absorption by sample is directly measured from the difference in intensity between two beams.

Mirrors are used to reflect the two beams to a light chopping instrument named as optical chopper. It rotates at a certain speed, and reflects both the sample and reference beam to monochromator. Monochromator contains a grating mirror that transforms the polychromatic light into the monochromatic light. Monochromator gradually rotate and focus the monochromatic reference beam as well as sample beam into the detector. The detector working mechanism

depends on the principle of thermocouple. The thermocouple detector alters the thermal energy into electrical energy. When the specimen absorbed radiation of a specific frequency then the detector will obtain a strong reference beam and the weak sample beam that results in an alternating current. An amplifier amplifies the signal and a recorder records the absorption bands. IR spectrum is therefore achieved in the form of a plot of absorption against wavenumber [66, 67].

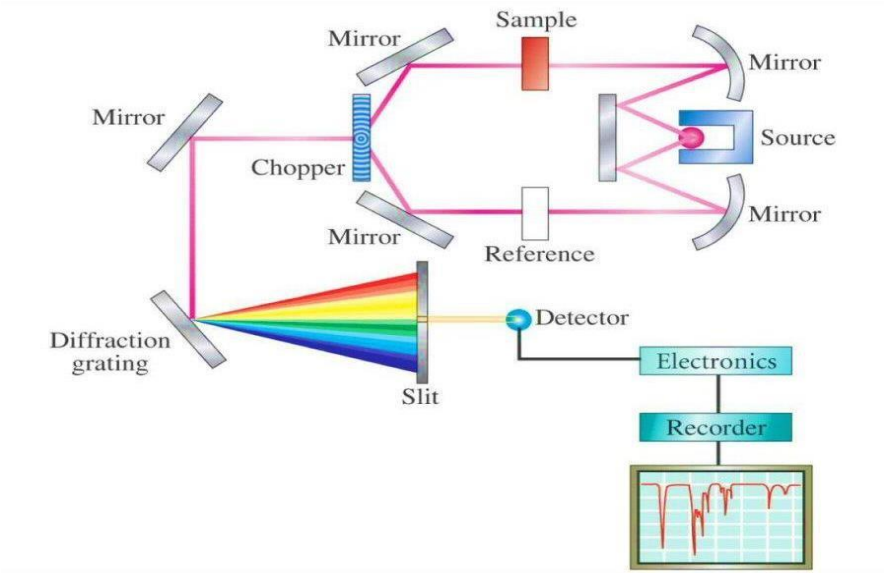

Figure 3.6 FT-IR spectrophotometer

Applications:

- IR spectroscopy is used in the determination of number and nature of bonds in a compound.
- It is used to identify functional groups existing in compound under analysis.
- It helps in the determination of configuration of organic compounds via correlation and analysis of spectra.
- Contaminations in the particular compounds can be identified with IR spectroscopy.
- IR spectroscopy is also employed to discover the percentage composition of a mixture of compounds.
- IR spectroscopy is also used to regulate the development of reaction.

3.2.3. Scanning Electron Microscopy (SEM)

Scanning electron microscopy (SEM) is an exceptional analytical technique used for surface analysis of different materials by employing focused beams of electrons. It is very powerful device for identification and examination of contamination in samples, imperfections and unidentified particulates. Topography, configuration and morphology of sample become clear through the greatly resolved three-dimensional images with the magnification of ~X50, 000.
Dr. Charles Oatlev and his students established Scanning Electron Microscope in 1950, which is a type of an electron microscope. Its working mechanism is same as of light microscope on the other hand for the magnification electron beam is used instead of the photons. An electron gun generates the beam of energetic electron positioned at the top of device [68, 69]. Main components of scanning electron microscope are schematically illustrated in Fig. 3.7.

Usually two kinds of guns are used for the generation of electrons named as “Thermionic gun and Field emission gun”. Thermionic gun heats up the filament that heated filament ejects electrons on the other hand use of electrical field for the purpose of electron emission is performed via Field emission guns. Number of these electrons directly influence the magnification.

Scanning electron microscopes involves a number of electromagnetic lenses for leading electrons from the column towards the sample. These lenses are positioned in the vacuum chamber and are present in the form of tube enclosed in coil generally named as “solenoids”. Solenoids are lineup to focus the beam of electron. These arrangements cause fluctuations in voltages and thus an increase or decrease in the speed with which electrons strike the sample surface. Sample section comprises sample platform for the steady support of samples. SEM sample stage displays horizontal as well as vertical tilting (T), rotation (R) and movement (X, Y).

> Field of view is thus designated by X and Y movements whereas Z and T movements support to regulate resolution and also the depth of focus.

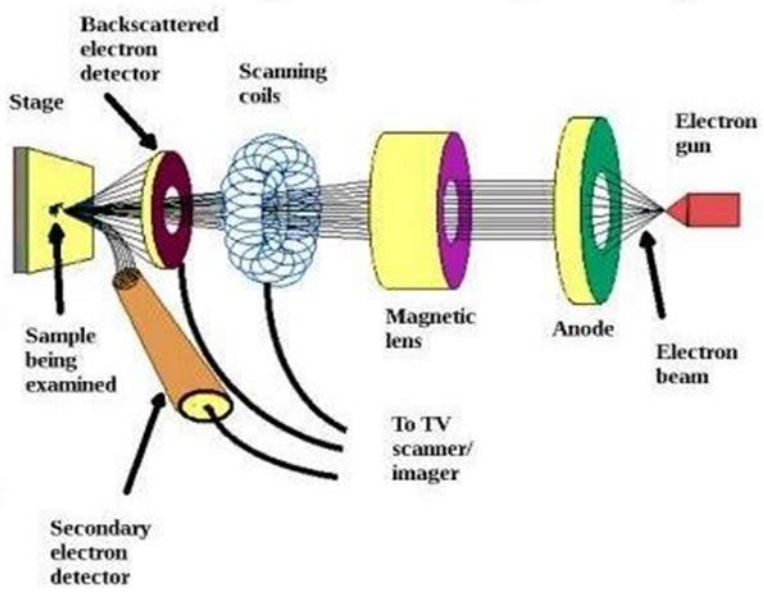

Figure 3.7: components of scanning electron microscope

Recently automatic sample stage is used which can be attuned simply via mouse. Incident ray of electron striking the sample surface, x-rays as well as three dissimilar types of electrons are emitted from the sample surface [70]. **Fig 3.8** is schematic illustration of various electron beams formed when interaction of incident beam with sample occurs. Secondary electron detector, backscatter detector, diffracted backscatter detector and x-ray detector are various kinds of detectors used for the detection of various scattered electrons. The sensitivity of certain secondary electron microscope relies on the kind of detectors it embraces. Backscattered electrons aid in the determination of differences in multiphase sample whereas secondary electrons provide information of topography and sample morphology [71]. Interaction of incident beam of electron interacts with surface of sample results in discharge of electrons from sample surface. The images attained by interaction provide information about sample size, shape and composition.

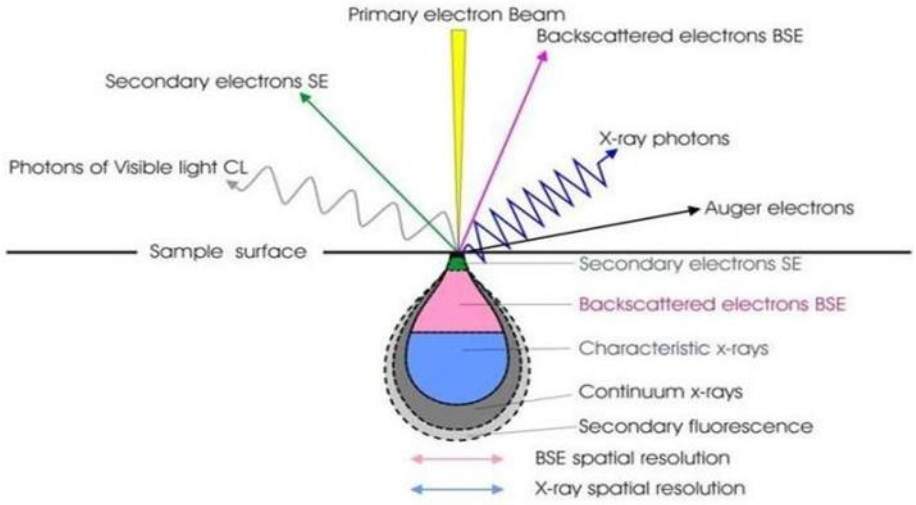

Figure 3.8: interaction of incident electron beam with sample surface

Scanning Electron Microscopy (SEM)/Energy Dispersive X-Ray Analysis (EDX)

SEM in combination with an Energy Dispersive X-Ray Analyzer is used to offer high- resolution images to analyze elements both in and on the sample surface and examination of sample semi-quantitative elemental composition. It is also used to for the detection of metal coatings and external particles. From "10 mm × 10 mm to ~ 1 μm × 1 μm", area can be analyzed by SEM/EDX and image resolution is from mm to ~50 nm.

EDX detector usually filters the particular x-rays of numerous elements into an energy spectrum that is analyzed to find the quantity of the specific element. Energy spectrum is shown in the form of a graph between energy and X-ray counts.

Applications:

SEM/EDX is usually used for the investigation of topography, morphology, and composition of the interested sample. Additionally, impurities, interphase studies, surface defects, alterations in chemical compositions and crystal structure identification can also be determined using SEM.

SEM/EDX is also used in most of the industries like ceramic, semiconductors, automotive, material, minerals, health devices, and medicine for quality control and compositional investigation of the products [69].

3.2.4. UV-Visible and UV-Vis Diffuse Reflectance Spectroscopy (DRS)

UV-Vis diffuse reflectance spectroscopy works on the similar basic principle of UV-Vis spectroscopy and is used to observe optical properties of powdered samples. UV-Vis spectroscopy is an electronic spectroscopy because it includes the promotion of electron from the ground state to the higher energy state. For ultraviolet region the electromagnetic radiation wavelength ranges from 10 nm to 400 nm while for visible region from 400 nm to 800 nm. In both regions' absorption of electromagnetic radiation by a molecule works on same principle therefore they are collectively named ultraviolet-visible spectroscopy.

When electromagnetic radiations of required wavelength is absorbed by the molecules then electronic transition occur from the highest occupied molecular orbital having low energy to the lowest unoccupied molecular orbital having high energy. The wavelength of absorbed radiation depends on the energy difference between already occupied orbital and the orbitals to which electrons are promoted. Mostly, a number of transitions occur that result in the establishment of numerous bands in absorption spectrum, which is named as UV/Vis spectrum. This spectrum offers interesting information of the tested molecule [72]. UV-Vis diffuse reflectance spectrum is a plot of percentage reflectance versus wavelength.

The device used for the measurement of absorption bands in UV/Vis spectrum is named as spectrophotometer or spectrometer. **Fig 3.9** is schematic illustration of components of UV/Vis spectrophotometer. The source of radiation is tungsten filament lamp and hydrogen-deuterium discharge lamp. The tungsten filament lamp offers radiation of wavelength more than 375 nm, which covers visible region whereas hydrogen-deuterium discharge lamp provides a radiation of wavelength below 375 nm, which covers ultraviolet region. Superior spectrometers have the capability to measure up to a short wavelength of about 185 nm. On the other hand, ordinary spectrometer cannot measure accurately below 200 nm in the UV region.

For investigation below wavelength of 200 nm the entire path is made evacuated. This region of below 200 nm is named as vacuum ultraviolet region. The ultraviolet radiations are reflected through the solenoid mirror toward the monochromator. A monochromator comprises of prism, entrance slit, exit slit and mirrors to deflect the radiations. Monochromator convert polychromatic light to monochromatic light via prism.

Beam splitter is used to split the monochromatic beam into the two beams of the same intensity. One beam passes over sample cell while the other beam passes through the reference cell. Sample cells are typically rectangular having a path length of about 1 cm. For low concentration samples the longer path length cells are usually used. Sample cells are generally made up of quartz as quartz is transparent in both the region of UV/Vis. Glass sample cell is not usually used as it display strong absorption in the UV region. Both reference cell and sample cell are used in the double beam spectrometer having identical path length and transmit radiation of same range.

Typically scanning of samples occurs in the very dilute solutions. One milligram of a compound under examination is perfectly weighed following the dissolution in appropriate solvent to make a solution up to 100 ml. For the exposure of sample to radiation a little amount of this solution is taken in a sample cell to. The absorption by sample is calculated from difference between the intensities of reference cell beam and sample cell beam at each wavelength. This difference is calculated either by ratio recording technique or optical null process.

At that point the two beams are reflected toward the optical chopper. It comprises of rotating semicircular mirror rotating at a frequency of about 10 cycles per second. The reflection of chopper causes the reflectance of both the reference beam and the sample beam towards the detector. The most commonly used detectors in spectrometers include phototubes and photomultiplier tubes. Photomultiplier tube is used in the double beam instrument as it can detect lower intensity radiation than phototube. At the certain instant, the beam impacting on the detector is either sample beam or reference beam. After the absorption of light, the sample beam intensity is lowered. As a result, the detector accepts a powerful beam from the reference cell and a weak beam from a sample

cell. The detector here is working as thermopile therefore the combination of intense and weak beam results in generation of electric current flowing from the detector towards the amplifier. The amplifier in UV/Vis spectrum is used to amplify merely the alternating current in the detector. The ratio of the intensities of the sample beam and reference beam is amplified and transferred to a self- balancing potentiometric recorder. The recorder accepts the amplified ratio approaching from the amplifier. The recorder records the absorbance against wavelength. The graph hence attained is called UV/Vis spectrum [72-74].

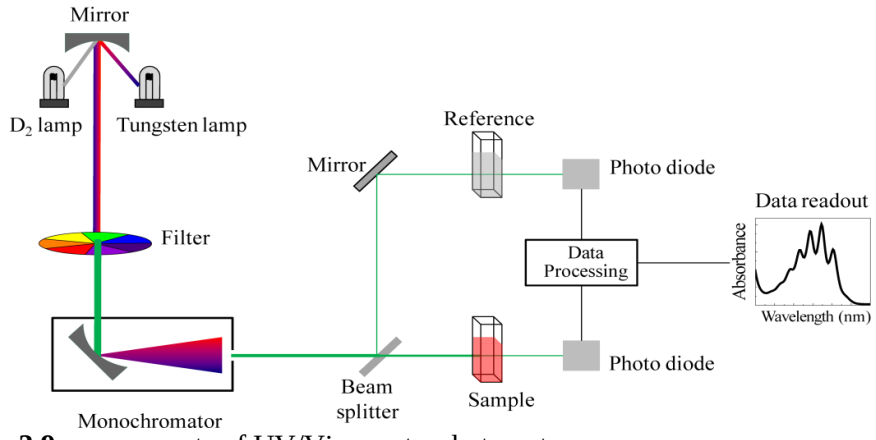

Figure 3.9: components of UV/Vis spectrophotometer

Applications:

Most significant applications of UV/Vis spectroscopy include [73].

- The determination of structure and functional group of a compound.
- It can also be used to determine ionization constant.
- Rate of reactions that include a change in absorbing group can be determined by UV/Vis spectroscopy.
- Stereo-chemical information of definite molecules can be determined by using UV/Vis spectroscopy.
- It aids to differentiate between conjugated and non-conjugated system and gives information about extent of conjugation.
- UV/Vis spectroscopy is also used to detect impurities

3.2.5. Dielectric Characterization

For dielectric characterization, the following properties of samples are tested.

Dielectric constant

Dielectric constant is calculated using relation 3.1.

$$\varepsilon' = \frac{\varepsilon^{\circ} \times D}{C \times A} \qquad (3.1)$$

Dielectric Loss

Dielectric loss is calculated using relation 3.2.

$$\varepsilon^{JJ} = \varepsilon^{J} \times D \qquad (3.2)$$

Tangent Loss

Tangent Loss is calculated using relation 3.3.

$$\delta = \frac{\varepsilon''}{\varepsilon'} \qquad (3.3)$$

AC Conductivity

AC conductivity is calculated using relation 3.4.

$$\sigma = 2\pi f \varepsilon^{\circ} \varepsilon'' \qquad (3.4)$$

LCR meter is an electronic device that accurately measures resistance capacitance and inductance at different frequencies with high precision. LCR meter is used in two configurations for the measurement of impedance.

Current-voltage method: This method is used to analyze dielectric properties at high frequencies. In this method two distinct measurement alignments are used for low and high impedance circuits (Figures 3.10 and 3.11)

LCR meter is an electronic device that accurately measures resistance capacitance and inductance at different frequencies with high precision. LCR meter is used in two configurations for the measurement of impedance.

Current-voltage method: This method is used to analyze dielectric properties at high frequencies. In this method two distinct measurement alignments are used for low and high impedance circuits (Figures 3.10 and 3.11).

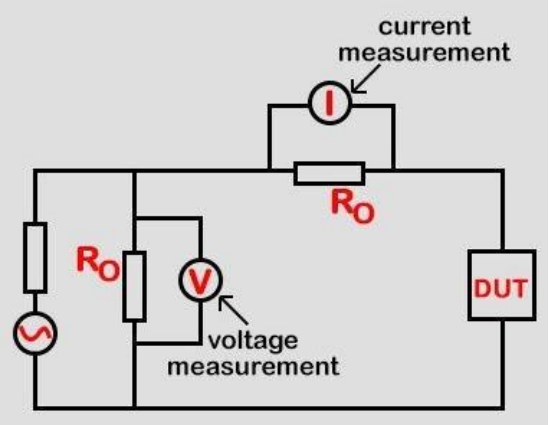

Figure 3.10: Current-voltage configuration for high impedance circuits [75]

Bridge method: This method is useful for the evaluation of dielectric properties at low frequencies up to 100 kHz. The method is based on Wheatstone Bridge principle (Figure 3.12). In the bridge circuit device to be examined is positioned. Following are the two impedances in the circuit

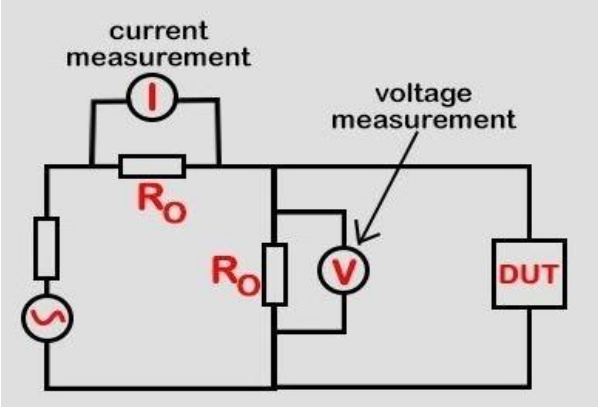

Figure 3.11: Current-voltage configuration for low impedance circuits [76]

named as Z2 and Z4. When current stops flowing in the other unknown impedance device (Z1); impedance of device under investigation (DUT) is determined by the following relation.

$$Z1/Zu=Z2/Z4$$

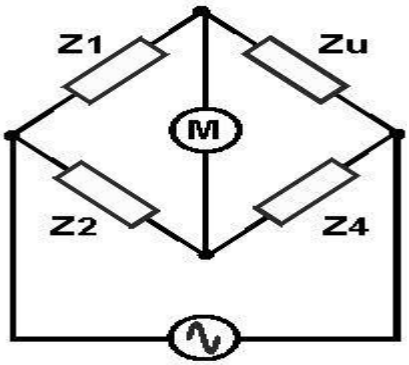

Figure 3.12: Bridge method circuit diagram [76]

Chapter 4- Results and Discussion

4.1. Characterization of ZnO:

4.1.1. SEM Analysis of ZnO:

To determine the mrphology of the prepared ZnO particles scanning electron microscopy was performed. Scanning electron micrographs of ZnO are shown in the figure **4.1**. It can be clarely seen in figure 1a that ZnO particles are in the form of flowers and they are homogenous in shape throughout the sample. The diameter of the flower was also measured with radius of 74.46 nm.

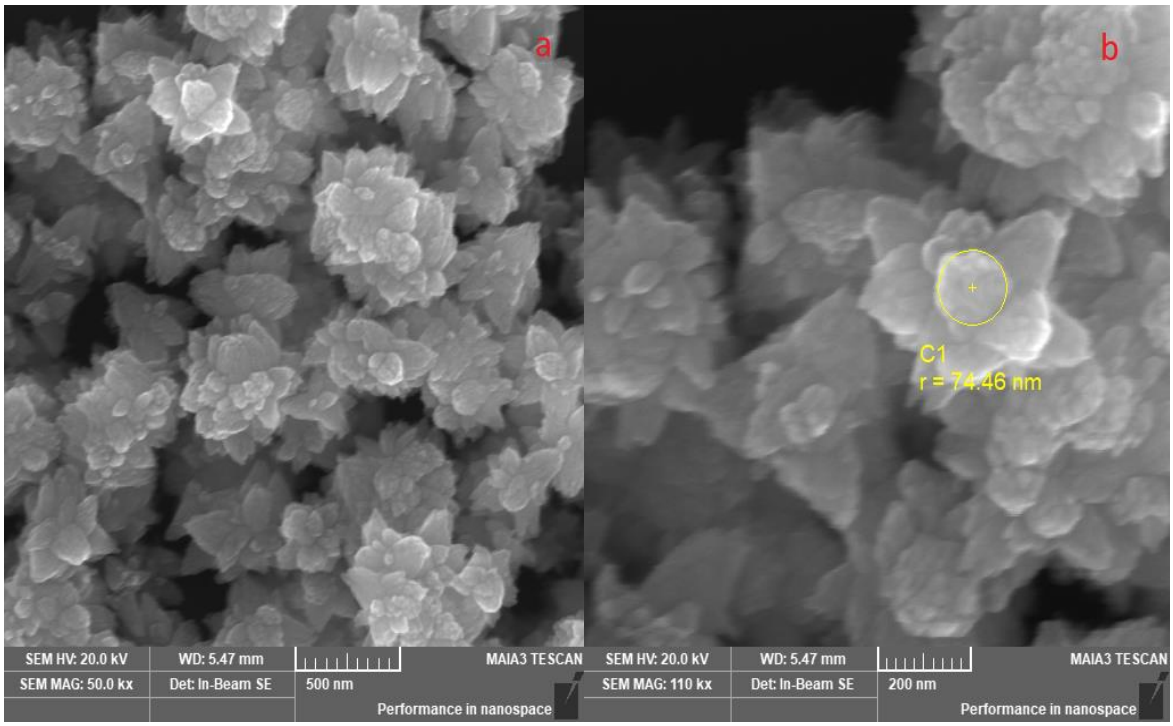

Figure: 4.1. SEM images of ZnO

4.1.1.1. SEM Analysis of ZnO@ Fe_3S_4 Composites:

Morphology of ZnO@ Fe_3S_4 x=(0.6, 0.8, 1, 1.2, 1.4) was determined by scanning electron microscope. Scanning electron micrographs of ZnO@ Fe_3S_4 of all the sample is shown in the figure **4.2**. Here we can see that Fe_3S_4 is in the form of thick sheet and the flower morphology of ZnO particles is converted into these sheets as well and well embedded in these amorphous sheets that's why some peaks are missing in figure XRD of ZnO.

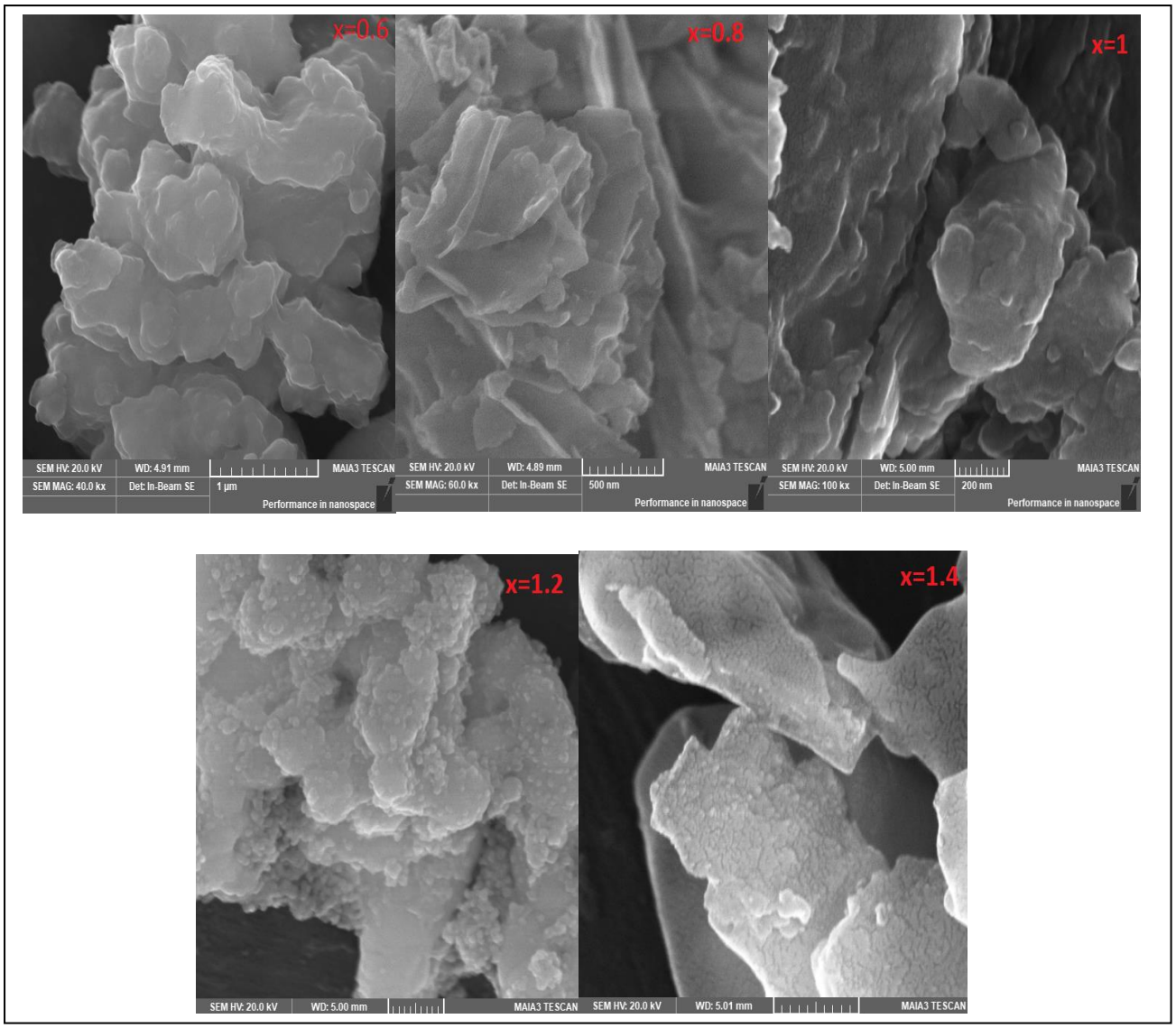

Figure: 4.2 SEM images of ZnO@ Fe_3S_4 Composites

4.1.2. XRD analysis ZnO:

The XRD patterns as-prepared of ZnO were shown in figure **4.3**. The Nano-crystalline single phase of ZnO was synthesized by the Polyol method and was confirmed by powder XRD measurements. The powder XRD pattern of the sample shows the crystalline nature of the ZnO having *hexagonal* wurtzite structure (matched with JCPDS No. 36-1451) with space group of **P63mc**

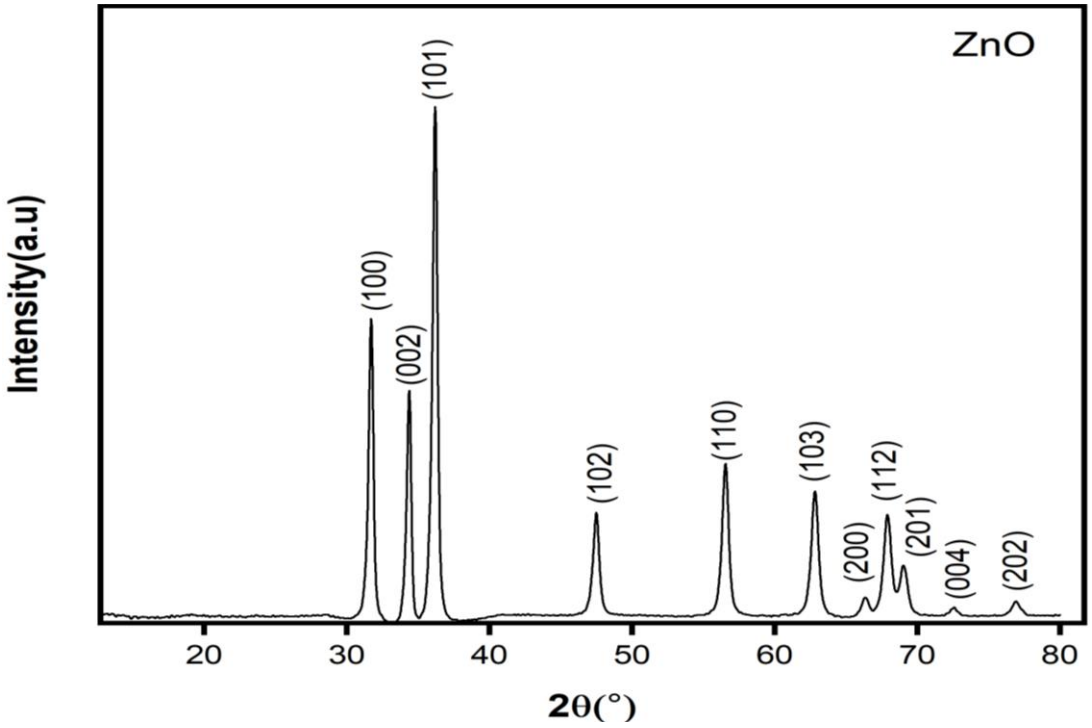

Figure: 4.3. XRD pattern of ZnO

All the diffractions peaks of ZnO can be indexed into **(100), (002), (101), (102), (110), (103), (200), (112), (201), (004) and (202)**. This structure is basically hexagonal closed packed structure. In this hexagonal closed packed unit cell, the Zinc cations are in +2 state while Oxygen anions are in -2 state. So, there is only one Zn^{+2} cation for one O^{-2} anion in the lattice to neutral each other electrically.

Using the value of Full width half maximum (FWHM (β)) of the diffraction peak, the crystallite size was calculated through Debye-Scherer formula:

$$D = \frac{k\lambda}{\beta cos\theta}$$

Where ‘D’ is crystallite size, ‘k’ is Scherer constant (.9), ‘λ’ is the X-ray wavelength, β is the full width half maximum FWHM and θ is the Bragg’s angle. The average calculated crystallite size of pure ZnO was found to be 19.29 nm.

From XRD pattern of ZnO the lattice parameters were also calculated which are given in the table1

S.No	Sample name	Lattice parameter a=b (Å)	Lattice parameter c (Å)	Cell volume	Particle size
1	ZnO	3.251552	5.214687	47.74636	19.29nm

Table no 4: lattice parameters of ZnO

4.1.2.1. XRD analysis of ZnO@ Fe_3S_4 Composites:

In XRD pattern of composite samples the ZnO peaks are reproduced accompanied with additional peaks of Fe_3S_4 which corresponds to the greigite phase as shown in the figure **4.4**. the dominenet planes of the greigite phase in the all the samples are (220), (311), and (440) while there is only extra peak 28.5° corresponds to FeS_2 pyrite phase.

In the composite samples the intensity of ZnO peaks are suppressed by the Fe_3S_4 greigite phase which completely wrap up the ZnO particles. As the concentration of Fe_3S_4 increases peak at 63° also get vanished in A12 and A14 samples.

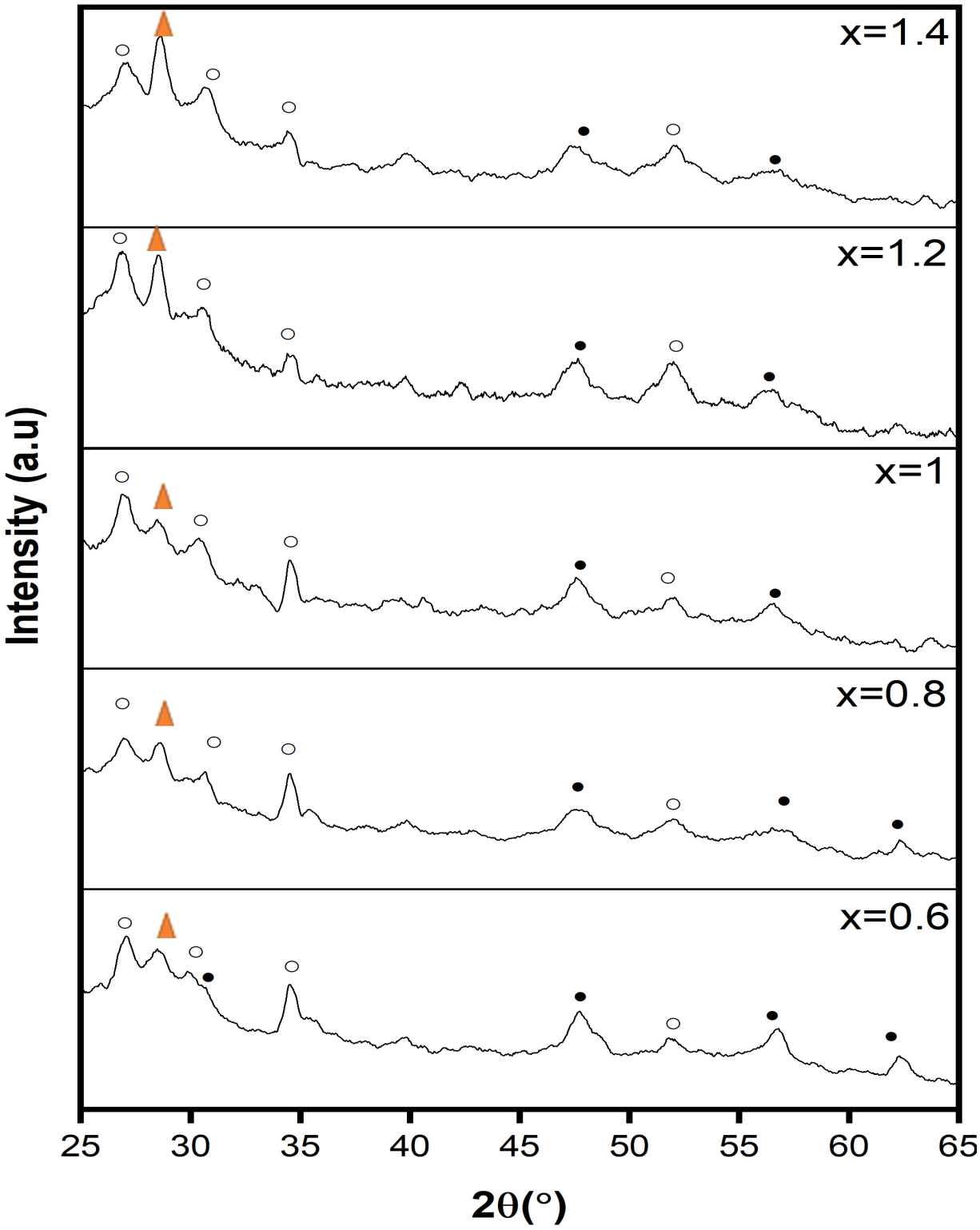

Figure 4.4: XRD pattern of ZnO/ Fe_3S_4

Lattice parameters were calculated for the composite samples and it was observed the as the concentration increases the peaks of ZnO shift towards higher angle.

S.No	Sample name	Lattice parameter a=b (Å)	Lattice parameter c (Å)	Cell volume	Particle size
1	A6	3.24098	5.191	47.2275	12.407 nm
2	A8	3.242719	5.193	47.2916	16.386 nm
3	A11	3.245711	5.207	47.5121	16.697 nm
4	A12	3.248341	5.222	47.7189	18.468 nm
5	A14	3.267207	5.224	48.2933	18.084 nm

Table 5: lattice parameters of ZnO/ Fe_3S_4

4.1.3. **FTIR analysis of ZnO**:

Fourier transform infrared spectroscopy analysis was done to confirm the Zn-O bond formation. Figure 4.5 shows the FTIR spectrum of ZnO nanoparticles in the range of 4000 - 400 cm^{-1} wavenumber. Due to absorption of water molecules the absorption at high frequency region at 3310 cm^{-1} is observed which can be assigned to the stretching vibration of O-H· The peaks at 1150 **cm^{-1}** and 1023 **cm^{-1}** can be assign to the C-O and Zn-OH bonding. The absorbance peak at 872 **cm^{-1}** is related to Zn-C which might be due to deposition of carbon on the surface of ZnO during annealing. Peak at 491 **cm^{-1}** confirms the formation Zn-O bonding [77].

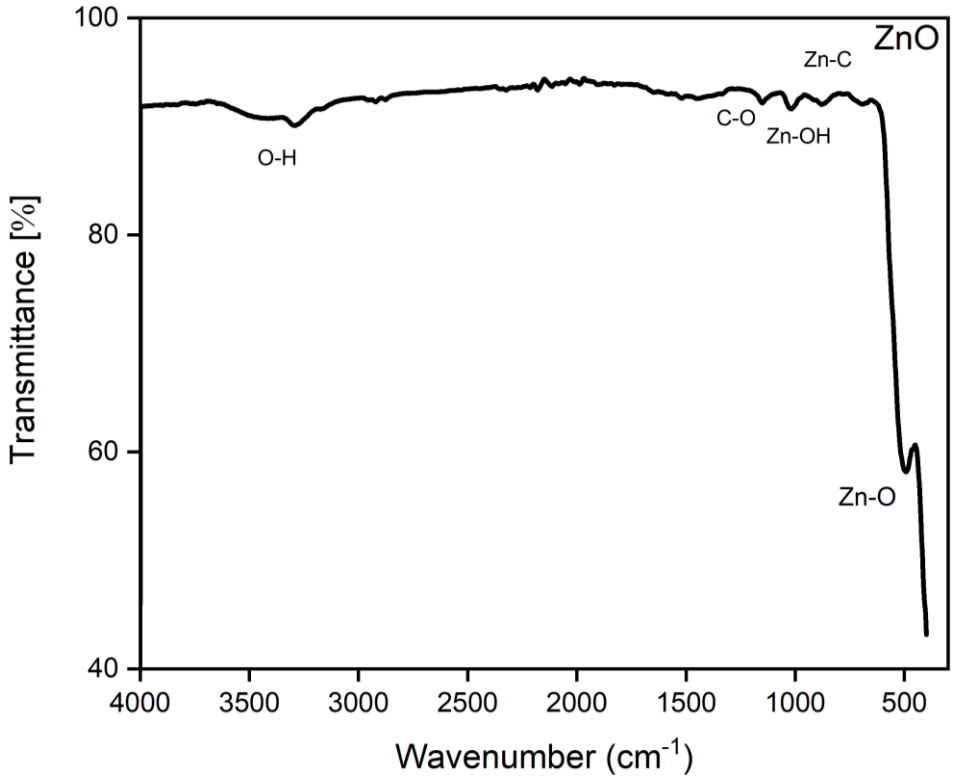

Figure 4.5. FTIR pattern of ZnO

4.1.3.1. FTIR analysis of ZnO@ Fe_3S_4 Composites:

FTIR spectrum of synthesized composites of ZnO with Fe_3S_4 (x=0.6, 0.8, 1, 1.2, 1.4) are shown in the figure **4.6**. The curve band at 3300 **cm^{-1}** shows a little moisture (O-H) in the samples. The band at 1414 **cm^{-1}** can be assigned to the stretching band of C-H from ethylene diamine during synthesis. Two bands appeared at 1184 **cm^{-1}** and 1018 **cm^{-1}** can be assigned to the stretching vibration of Fe=S. the obscure bands at 746 **cm^{-1}** and 639 **cm^{-1}** can be assigned to Fe-S and S-S bonds.in the finger print region or in the low frequency region[78]. the appeared peaks at 497 **cm^{-1}** and 454 **cm^{-1}** are related to Zn-O bonding.

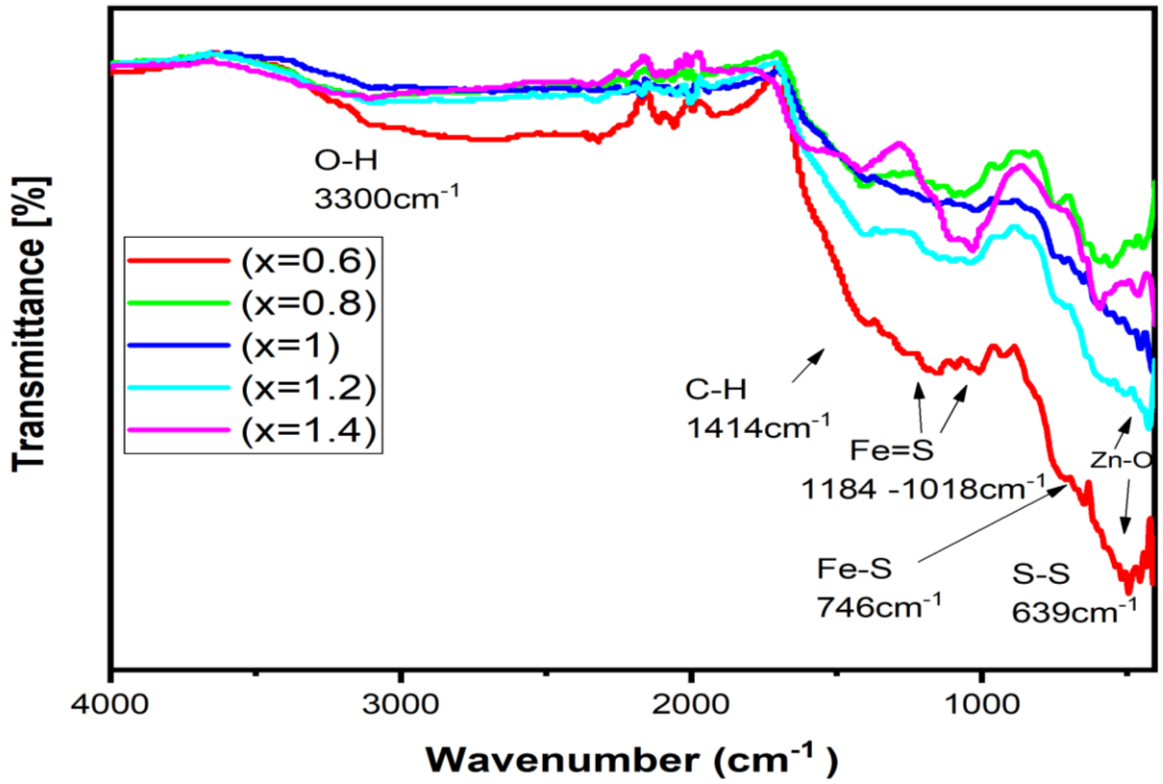

Figure 4.6 FTIR pattern of ZnO/ Fe_3S_4

4.1.4. Ultraviolet-Visible Diffuse Reflectance Spectroscopy of ZnO and ZnO@ Fe_3S_4

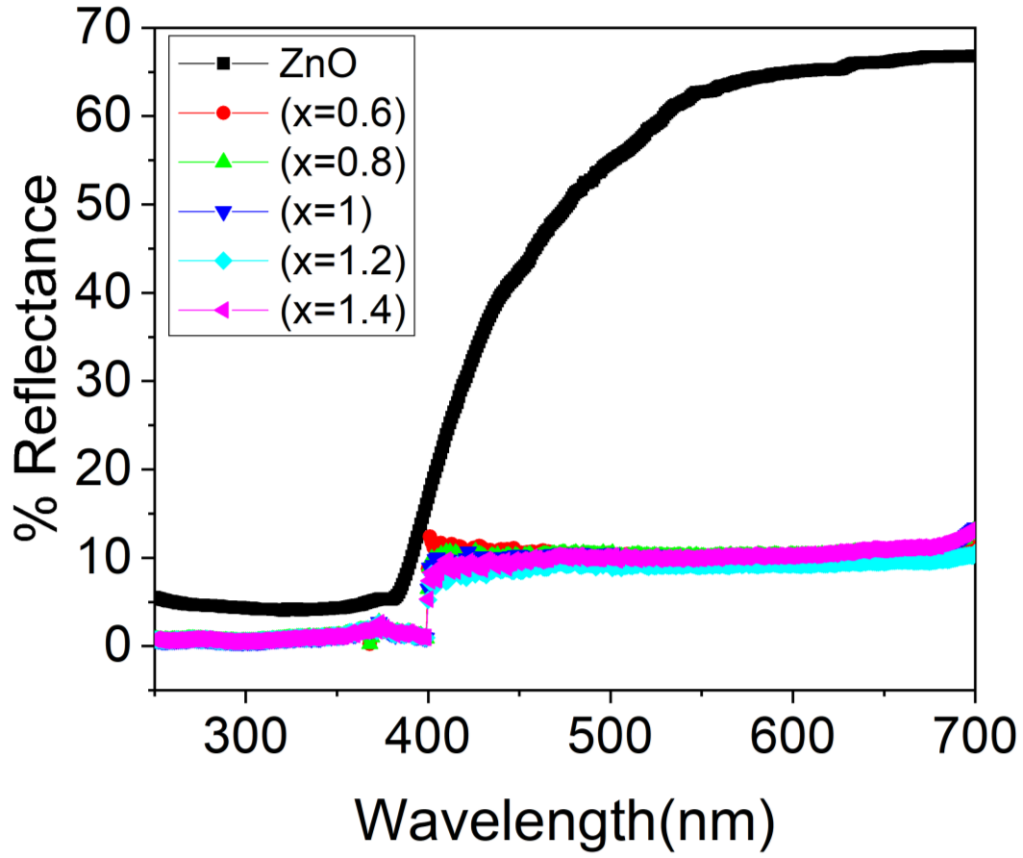

Figure 4.7 UV/Vis reflectance spectrum of ZnO and ZnO–$(Fe_3S_4)_x$ x (=0.6, 0.8, 1, 1.2, 1.4)

Figure 4.7 shows the optical properties of ZnO and ZnO–Fe_3S_4 nanocomposites which were investigated using UV-vis diffuse reflectance spectra. It can be seen that the ZnO nano flowers shows only absorption peak at 393 nm in the ultraviolet region, which can be assigned as a characteristic absorption peak of ZnO. While after addition of Fe_3S_4 nanosheets which wrapped around the surface of ZnO structure, absorption peaks shift toward higher wavelength. All these composite shows absorption in the same region (350 -700).

ZnO band gap was calculated via Tauc plot as shown in inset of **Figure 4.8** Reflectance factor, F(R) was utilized rather than absorption factor in UV DRS and calculated via Kubelka-Munk expression as shown in equation (1).

$$(R)=(1-R)^2/2R= K/S \qquad (1)$$

Where R is absolute reflectance, K is Molar absorption co-efficient and S is scattering coefficient. Optical Band gap of ZnO was determined to be 3.35eV by means of Tauc plot as shown in inset of **figure 4.8.**

The band gap of ZnO-Fe_3S_4 nanocomposites obtained from Kubelka–Munk function plot is estimated to be 3.05 eV for sample A6 and A8 and 3.06 eV for all the remaining samples. These results indicate that coupling of Fe_3S_4 with ZnO narrowed the band gap of ZnO.

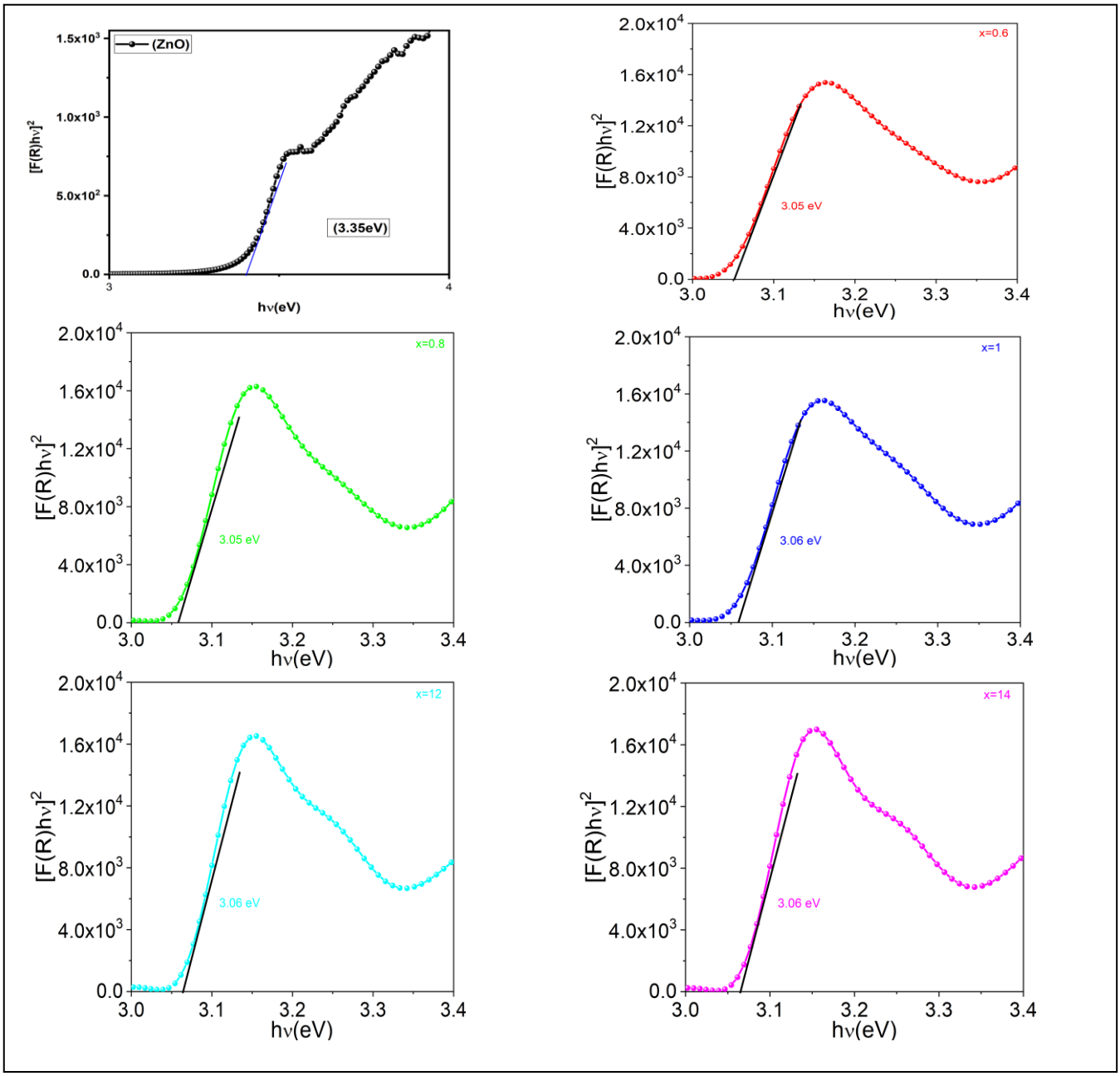

Figure **4.8** band gap/Tauc plot of ZnO and ZnO–$(Fe_3S_4)_x$ x (=0.6, 0.8, 1, 1.2, 1.4)

4.1.5. Dielectric Behavior

4.1.5.1. Dielectric Constant and Dielectric Loss

Real part of permittivity ε' can be defined as the energy stored in dielectric materials and represents the strength of dipoles alignments. while imaginary part of it ε" represents the energy dissdipated in dielectric materials or simply known as the loss factor. Both the real and imaginary parts of permittivity represents total polarization of dielectric materials. Total polarization is the sum of the space charge polarization, which is defined by the space charge carriers, the hopping of charge carriers and the resultant displacement of charge carriers between localized states [79]. The dielectric properties of the synthesized nanocomposites powder were studied by making pellets from them. Firstly, the dielectric constant and the dielectric loss were calculated using the values obtained from the LCR meter and were plotted against the logarithm of frequency. The trends are shown in **Figure 4.9** and **Figure 4.10**

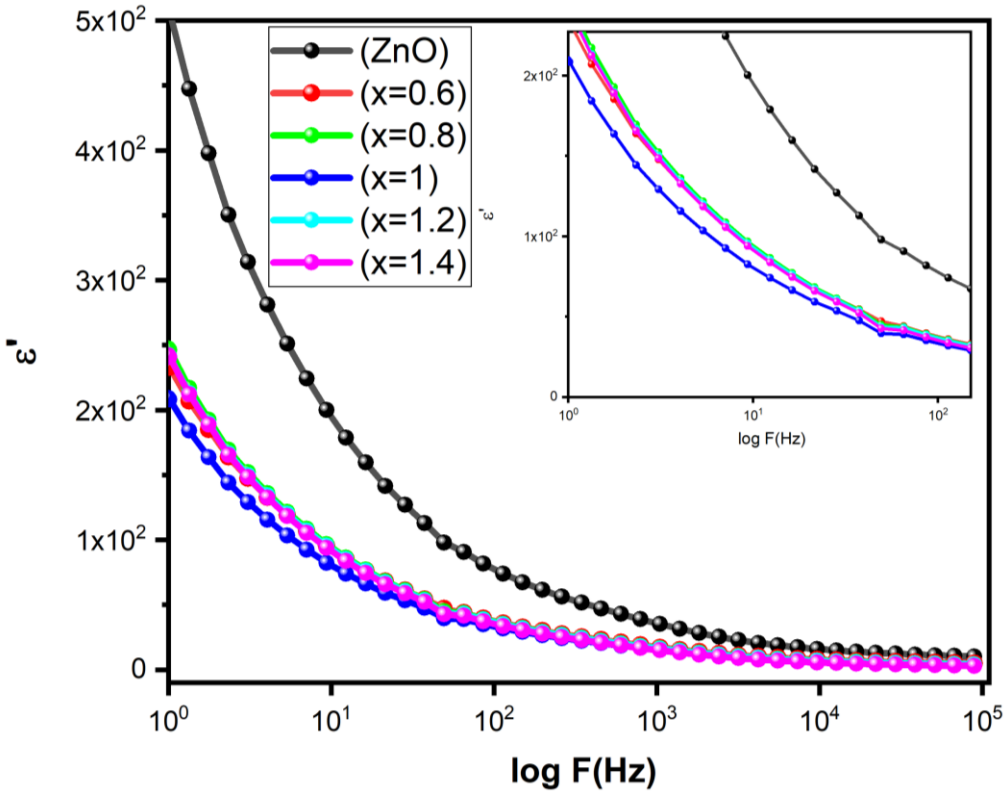

Figure 4.9: Dielectric constant

It is very hard for the applied filed to rotate the dipoles in its direction when they have strong interaction between them. The migration of electrons between two particles may cause the local displacement of charge carriers thereby producing dipoles, which determines polarization in

the system. Figure 4.9 shows the real part of dielectric constant ε' as a function of log frequency. At low frequency the dipoles follow the external alternating frequency. As the frequency increases the dipoles slowly lag behind the alternating frequency. At very high frequency the dipole can no longer follow the alternating field due to which the magnitude of ε' for the all the composite samples decreases possibly due to reversing the direction of electron by increasing frequency. Due to which the possibility of reaching electron at grain boundary decreases and polarization gets reduced too.

On the other hand, the imaginary part ε" (shown in **figure 4.10)** also decreased significantly as compared to ε' yielding the feature of low loss and high storage capability in composite samples.

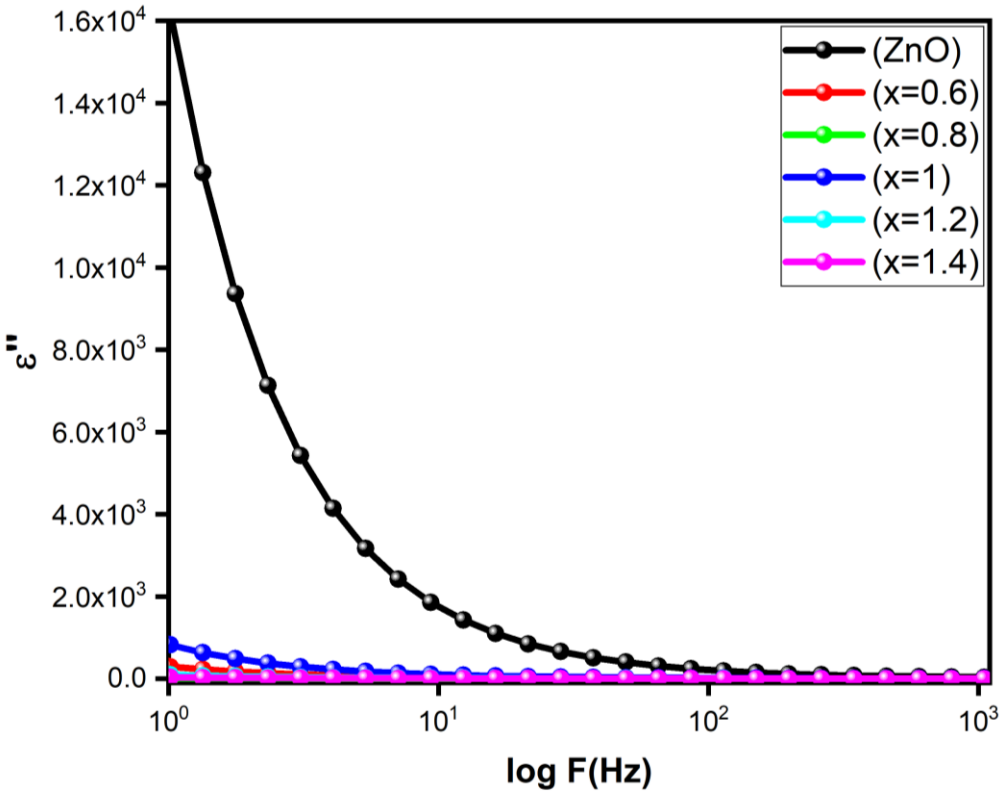

Figure 4.10: Dielectric Loss

4.1.5.2. Tangent Loss

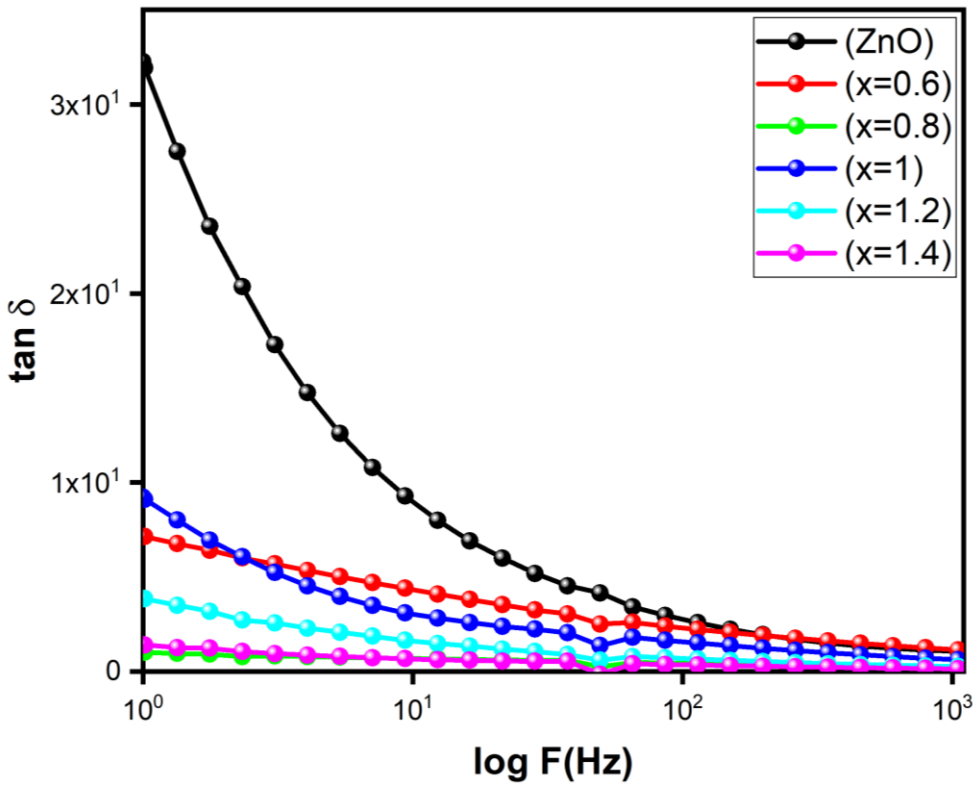

Figure 4.11: Tangent Loss

Tangent loss (tan **δ** = **ε'** / **ε''**) values as function of Logarithm of frequency for the nanocomposites are shown in **figure 4.11.** In the presence of external applied field, the amount of energy being dissipated in the samples can be represented by tangent loss. ZnO shows high loss as compared to its nanocomposite samples. As the frequency increases of applied field, the frequency of hopping electrons follows it but beyond certain value it doesn't follow as a result the loss gets decreased. Also, the formation of composite of ZnO with Fe_3S_4 change the conduction mechanism which is indicated by low loss. The tangent loss values get decreased with increased in concentration of Fe_3S_4. Except for A8 sample which might be due to inappropriate lattice defect. The property of decrease in tangent loss at high frequency enables them to high frequency devices.

4.1.5.3. AC Conductivity

Figure 4.12 shows variation in the AC conductivity with increase in external applied field. The AC conductivity values of ZnO and ZnO@ Fe_3S_4 (x=0.6, 0.8, 1, 1.2, 1.4) indicating insulating behavior at low frequency. With increase in the frequency of external applied field all the samples show increase in ac conductivity showing semiconducting behavior. The ac conductivity for composite samples tends to increase with increase in frequency as compared to pure ZnO showing dispersive behavior in the low frequency region, which might be due to re-orientation of dipole moments and conduction of mobiles charges within strictly localized states. The motion of these ions start disruption in the neighborhood. The composite samples show less conductivity as compared to pure ZnO which might be due to minimum interfacial recombination of ZnO and Fe_3S_4 layers at interface and charge transfers slowly between these two phases.

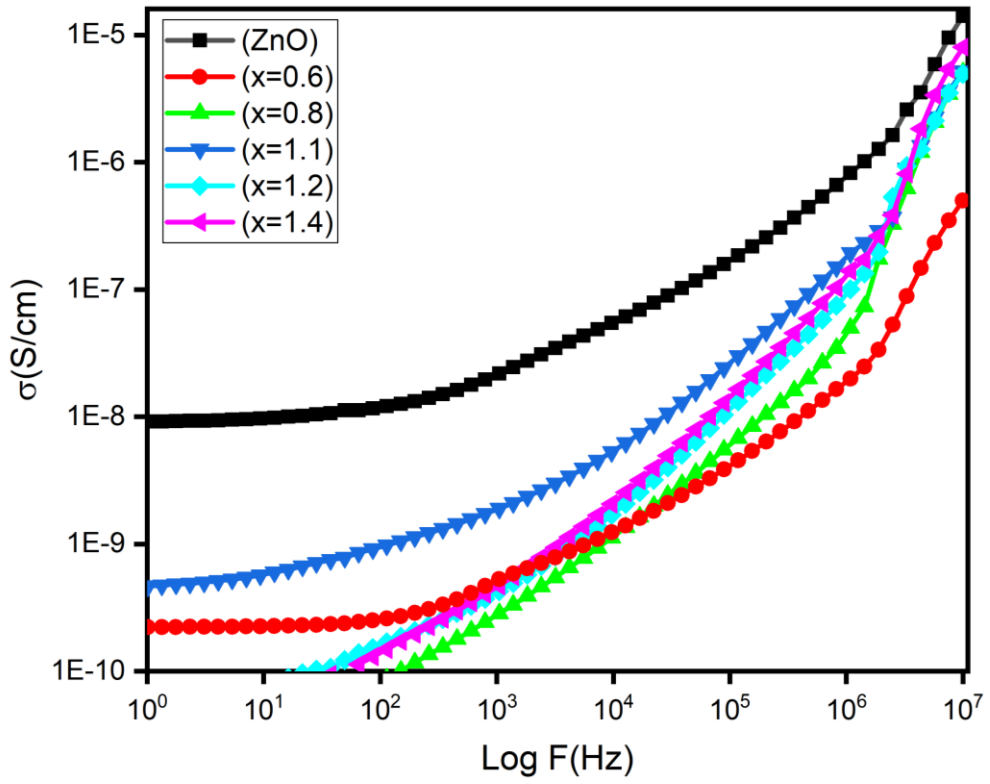

Figure 4.12: Ac conductivity

4.1.5.4. Impedance

Impedance measurements provide useful information about resistive and reactive impedance parts. Figure 4.13 is the representation of change in real part of impedance against logarithmic frequency at room temperature. It can be observed that impedance (Z) gradually decreases as frequency increases. With highest content of Fe_3S_4 (x = 0.8, sample A8), maximum value of (real) impedance is observed. Higher value of resistance corresponds to lower AC conductivity. This is in agreement with AC conductivity behavior illustrated in Figure 4.13.

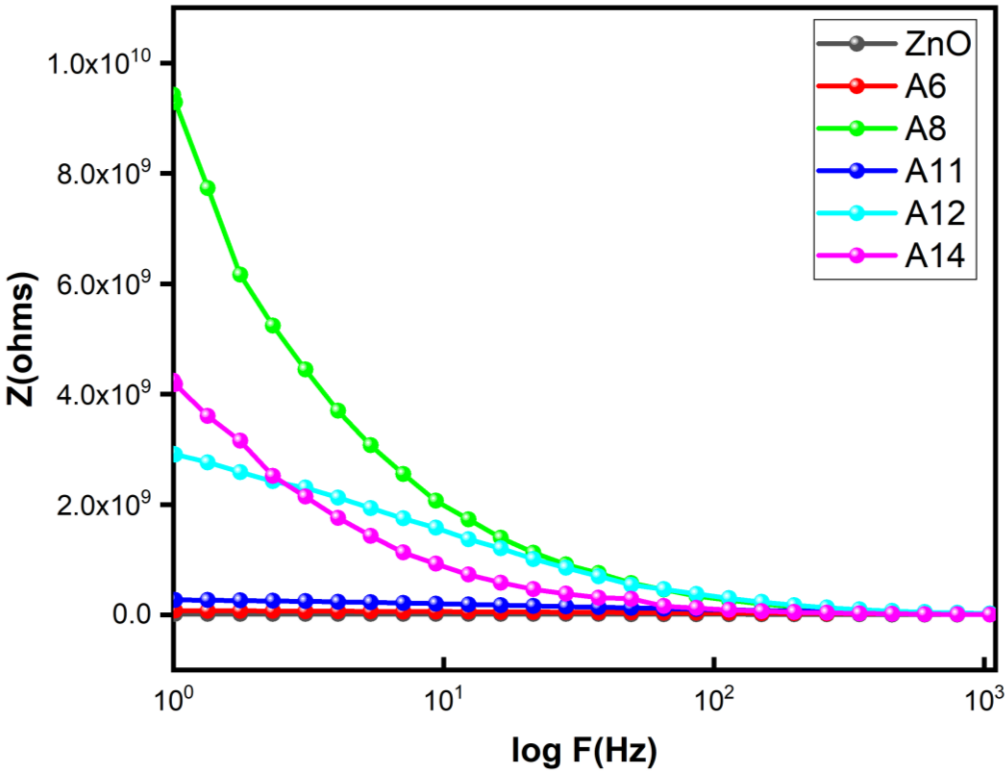

Figure:4.13 Impedance of ZnO@ Fe_3S_4

In other words, AC conductivity and impedance are inversely related. Cole-cole plot of ZnO@ Fe_3S_4 is shown in Figure 4.14. The imaginary impedance part is plotted against real impedance part. Ideally two semicircles are observed in cole-cole plots. The first semi-circle at lower frequencies represents resistance of grain boundaries, whereas resistance of grains is derived from the second semi-circle. Incomplete semi circles are evident from cole-cole plot of ZnO@ Fe_3S_4

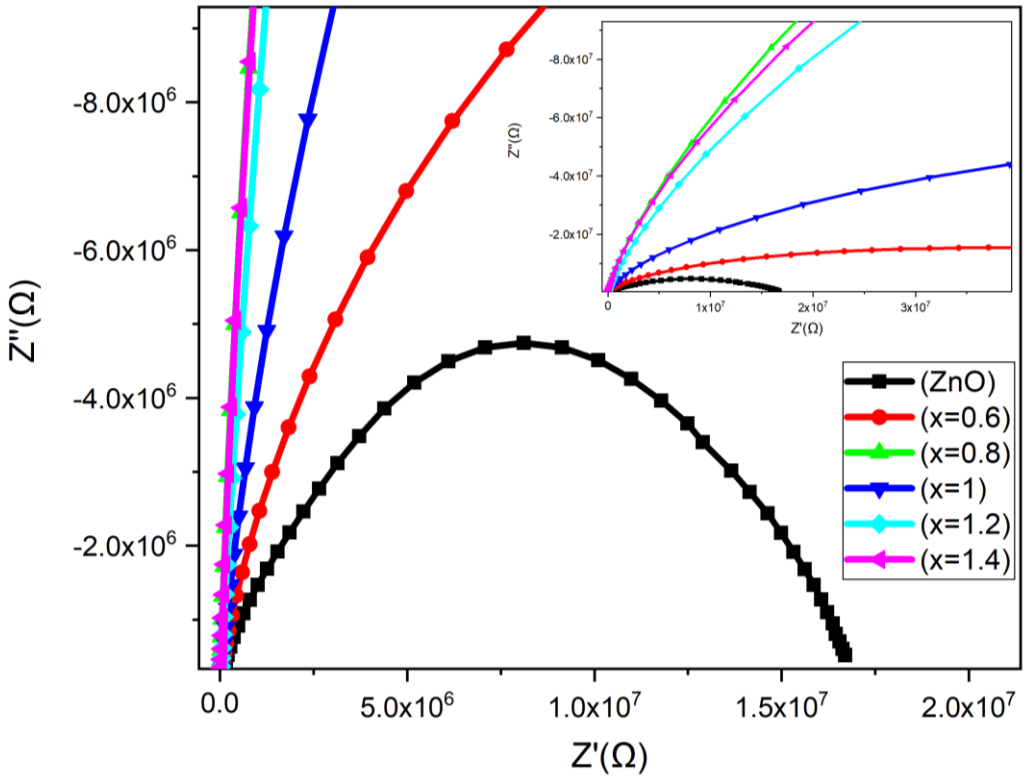

Figure:4.14 cole-cole of ZnO@ Fe_3S_4

Conclusion

ZnO and its composite with Fe_3S_4 were synthesized with five different ratio composition. The synthesis approach polyol method was adopted for the fabrication of pure ZnO. Later on, its composite was fabricated with Fe_3S_4 having different ratios x= (0.6, 0.8, 1, 1.2, and 1.4) in Teflon lined autoclave through solvothermal method. XRD identified the crystal structure of the prepared samples. The crystal structure of the pure ZnO was found to be hexagonal wurtzite. While in composite some of the peaks of ZnO and Fe_3S_4 or having low intensity, which is due to the amorphous nature of the composite material. the particle size of the composite material was gradually increasing from 12.4nm to 18nm as the Fe_3S_4 content increases while the particle size of ZnO was found to be 19 nm. For bond identification FTIR spectroscopy was done, where at 491cm^{-1} confirms the Zn-O bonding. While in composite material the bands at 1018 cm^{-1}, 746 cm^{-1}, 639 cm^{-1}, 454 cm^{-1} are related Fe=S, Fe-S, S-S and Zn-O respectively. Through SEM morphology of the samples was studied where pure ZnO nanoparticle was found to be in flower shape and these flower shapes were converted into thick sheets. UV-DRS gives us band gaps where ZnO band gap was found to be 3.35eV and this band gap was decreased to 3.06 eV in composite material.

Dielectric constant and dielectric loss depicted a decreasing trend with increase in frequency. Tangent loss also tends to decrease with the increasing frequency. AC conductivity of the samples showed an increasing trend with the increase in frequency. Impedance against logarithmic frequency at room temperature was observed where impedance (Z) gradually decreases as frequency increases.

Refrences

1. Hao, X.J.J.o.A.D., *A review on the dielectric materials for high energy-storage application.* 2013. **3**(01): p. 1330001.
2. Yao, K., et al., *Nonlinear dielectric thin films for high-power electric storage with energy density comparable with electrochemical supercapacitors.* 2011. **58**(9): p. 1968-1974.
3. Slenes, K.M., et al., *Pulse power capability of high energy density capacitors based on a new dielectric material.* 2001. **37**(1): p. 324-327.
4. Akagi, H.J.I.t.o.i.a., *New trends in active filters for power conditioning.* 1996. **32**(6): p. 1312-1322.
5. Lei, Q. and F.Z.J.I.t.o.p.e. Peng, *Space vector pulsewidth amplitude modulation for a buck–boost voltage/current source inverter.* 2013. **29**(1): p. 266-274.
6. Ishihara, T., et al., *Mixed oxide capacitor of CuO—BaTiO3 as a new type CO2 gas sensor.* 1992. **75**(3): p. 613-618.
7. Christen, T. and M.W. Carlen, *Theory of Ragone plots.* Journal of Power Sources, 2000. **91**(2): p. 210-216.
8. Du Pasquier, A., et al., *A comparative study of Li-ion battery, supercapacitor and nonaqueous asymmetric hybrid devices for automotive applications.* 2003. **115**(1): p. 171-178.
9. Wilk, G.D., R.M. Wallace, and J.J.J.o.a.p. Anthony, *High-κ gate dielectrics: Current status and materials properties considerations.* 2001. **89**(10): p. 5243-5275.
10. Winter, M. and R.J. Brodd, *What are batteries, fuel cells, and supercapacitors?* 2004, ACS Publications.
11. Kao, K.C., *Dielectric phenomena in solids*. 2004: Elsevier.
12. Maex, K., et al., *Low dielectric constant materials for microelectronics.* 2003. **93**(11): p. 8793-8841.
13. Ellabban, O., et al., *Renewable energy resources: Current status, future prospects and their enabling technology.* 2014. **39**: p. 748-764.
14. Varun, R. Prakash, and I.K. Bhat, *Energy, economics and environmental impacts of renewable energy systems.* Renewable and Sustainable Energy Reviews, 2009. **13**(9): p. 2716-2721.
15. Panwar, N., et al., *Role of renewable energy sources in environmental protection: A review.* 2011. **15**(3): p. 1513-1524.
16. Dincer, I.J.R. and s.e. reviews, *Renewable energy and sustainable development: a crucial review*. 2000. **4**(2): p. 157-175.
17. Liu, C., et al., *Advanced Materials for Energy Storage.* 2010. **22**(8): p. E28-E62.

18. Chu, S. and A.J.n. Majumdar, *Opportunities and challenges for a sustainable energy future.* 2012. **488**(7411): p. 294-303.
19. Simon, P. and Y. Gogotsi, *Materials for electrochemical capacitors.* Nature Materials, 2008. **7**(11): p. 845-854.
20. Coleman, J.N., et al., *Two-dimensional nanosheets produced by liquid exfoliation of layered materials.* 2011. **331**(6017): p. 568-571.
21. Dai, L., et al., *Carbon nanomaterials for advanced energy conversion and storage.* 2012. **8**(8): p. 1130-1166.
22. Bensebaa, F., *Clean energy*, in *Interface Science and Technology*. 2013, Elsevier. p. 279-383.
23. *https://www.wiley-vch.de/books/sample/3527407901_c01.pdf*.
24. Sharma, V.K., et al., *Silver nanoparticles: green synthesis and their antimicrobial activities.* 2009. **145**(1-2): p. 83-96.
25. Desilvestro, J. and O.J.J.o.t.E.S. Haas, *Metal oxide cathode materials for electrochemical energy storage: a review.* 1990. **137**(1): p. 5C.
26. Fernandez-Garcia, M., et al., *Nanostructured oxides in chemistry: characterization and properties.* 2004. **104**(9): p. 4063-4104.
27. Socratous, J., et al., *Electronic structure of low-temperature solution-processed amorphous metal oxide semiconductors for thin-film transistor applications.* 2015. **25**(12): p. 1873-1885.
28. Browne, M.P., et al., *Layered and two dimensional metal oxides for electrochemical energy conversion.* 2019. **12**(1): p. 41-58.
29. Sharma, A.P., et al., *Fabrication and characterization of SnO2 nanorods for room temperature gas sensors.* 2018. **8**(9): p. 095219.
30. Shen, G., et al., *Devices and chemical sensing applications of metal oxide nanowires.* 2009. **19**(7): p. 828-839.
31. Wei, X., et al., *A novel functional material of Co3O4/Fe2O3 nanocubes derived from a MOF precursor for high-performance electrochemical energy storage and conversion application.* 2019. **355**: p. 336-340.
32. Seliverstov, A., et al., *Molecular Metal Oxides for Energy Conversion and Energy Storage.* 2014: p. 217-242.
33. Wu, Y. and T. van Ree, *1 - Introduction: Energy technologies and their role in our life*, in *Metal Oxides in Energy Technologies*, Y. Wu, Editor. 2018, Elsevier. p. 1-16.
34. Mei, J., et al., *Two-dimensional metal oxide nanomaterials for next-generation rechargeable batteries.* 2017. **29**(48): p. 1700176.

35. Zemann, J., *Crystal structures, 2nd edition. Vol. 1 by R. W. G. Wyckoff.* 1965. **18**(1): p. 139-139.
36. Lucas, E., et al., *Nanocrystalline metal oxides as unique chemical reagents/sorbents.* 2001. **7**(12): p. 2505-2510.
37. Wang, Z.L.J.A.N., *Splendid one-dimensional nanostructures of zinc oxide: a new nanomaterial family for nanotechnology.* 2008. **2**(10): p. 1987-1992.
38. Pan, Z.W. and Z.L.J.S. Wang, *Nanobelts of semiconducting oxides.* 2001. **291**(5510): p. 1947-1949.
39. Özgür, Ü., et al., *A comprehensive review of ZnO materials and devices.* 2005. **98**(4): p. 11.
40. 46, *Luis Manuel Angelats "Silva Study of structural, electrical, optical and magnetic properties of ZnO based films produced by magnetron sputtering" PhD thesis, university of Puerto Rico UPR. (2006)*2006.
41. Hoffman, R.L., B.J. Norris, and J.F. Wager, *ZnO-based transparent thin-film transistors.* 2003. **82**(5): p. 733-735.
42. Bae, H.S., et al., *Photodetecting properties of ZnO-based thin-film transistors.* 2003. **83**(25): p. 5313-5315.
43. Izyumskaya, N., et al., *Preparation and properties of ZnO and devices.* 2007. **244**(5): p. 1439-1450.
44. Ryu, Y., et al., *Next generation of oxide photonic devices: ZnO-based ultraviolet light emitting diodes.* 2006. **88**(24): p. 241108.
45. Stolt, L., et al., *ZnO/CdS/CuInSe2 thin-film solar cells with improved performance.* 1993. **62**(6): p. 597-599.
46. Olorunyolemi, T., et al., *Thermal conductivity of zinc oxide: from green to sintered state.* 2002. **85**(5): p. 1249-1253.
47. Fan, Z., J.G.J.J.o.n. Lu, and nanotechnology, *Zinc oxide nanostructures: synthesis and properties.* 2005. **5**(10): p. 1561-1573.
48. Dal Corso, A., et al., *Ab initio study of piezoelectricity and spontaneous polarization in ZnO.* 1994. **50**(15): p. 10715.
49. Wang, Z.L.J.J.o.p.c.m., *Zinc oxide nanostructures: growth, properties and applications.* 2004. **16**(25): p. R829.
50. Guo, W., et al., *Gas-sensing performance enhancement in ZnO nanostructures by hierarchical morphology.* 2012. **166**: p. 492-499.

51. Kaviyarasu, K., et al., *Synthesis and Characterization Studies of Pb:Zr:/O2 Nanorods for Optoelectronic Applications.* 2017. **2017**: p. 1-3.
52. Zhang, Z., et al., *Controllable preparation of 1-D and dendritic ZnO nanowires and their large area field-emission properties.* Journal of Alloys and Compounds, 2017. **690**: p. 304-314.
53. Chou, T.P., Q. Zhang, and G.J.T.J.o.P.C.C. Cao, *Effects of dye loading conditions on the energy conversion efficiency of ZnO and TiO2 dye-sensitized solar cells.* 2007. **111**(50): p. 18804-18811.
54. Vikas, L.S., et al., *Vertically aligned ZnO nanorod array/CuO heterojunction for UV detector application.* 2014. **211**(11): p. 2493-2498.
55. Wang, L., et al., *Facet-dependent optical properties of nanostructured ZnO.* 2014. **147**(3): p. 1134-1139.
56. Laurenti, M., et al., *Surface Engineering of Nanostructured ZnO Surfaces.* 2017. **4**(2): p. 1600758.
57. Caruso, F.J.A.m., *Nanoengineering of particle surfaces.* 2001. **13**(1): p. 11-22.
58. Lam, K.-T., et al., *High-sensitive ultraviolet photodetectors based on ZnO nanorods/CdS heterostructures.* 2017. **12**(1): p. 1-7.
59. Xie Juan; , L.L., Xiong Cheng;, *Micronanoelectronic Technology Year 2017, Issue 1, Page 16-20,25,*2017.
60. Wang, X., et al., *CdSe nanoparticle-sensitized ZnO sheets for enhanced photocatalytic hydrogen evolution rates.* 2018. **747**: p. 826-833.
61. Fiévet, F., et al., *The polyol process: a unique method for easy access to metal nanoparticles with tailored sizes, shapes and compositions.* 2018. **47**(14): p. 5187-5233.
62. Watkin, D.J.J.C.R., *Chemical crystallography–science, technology or a black art.* 2010. **16**(3): p. 197-230.
63. Suryanarayana, C. and M.G. Norton, *Practical aspects of X-ray diffraction*, in *X-Ray Diffraction*. 1998, Springer. p. 63-94.
64. **Hebbar., K.R.**, ***Basics of X-Ray Diffraction and its Applications. I. K. International Publishing House Pvt. Limited***. **2007**.
65. Mirabella, F.M., *Modern techniques in applied molecular spectroscopy*. Vol. 14. 1998: John Wiley & Sons.
66. Stuart, B.J.K.O.e.o.c.t., *Infrared spectroscopy.* 2000.
67. Siesler, H.W., et al., *Near-infrared spectroscopy: principles, instruments, applications*. 2008: John Wiley & Sons.

68. Goldstein, J.I., et al., *Scanning electron microscopy and X-ray microanalysis*. 2017: Springer.
69. Reimer, L., *Electron scattering and diffusion*, in *Scanning Electron Microscopy*. 1998, Springer. p. 57-134.
70. Egerton, R.F., *Physical principles of electron microscopy*. Vol. 56. 2005: Springer.
71. Clarke, A., C. Eberhardt, and C.N. Eberhardt, *Microscopy techniques for materials science*. 2002: Woodhead Publishing.
72. Perkampus, H.H., *H.H. Perkampus: Encyclopedia of Spectroscopy, VCH, Weinheim, New York, Basel, Cambridge, Tokyo, ISBN 3-527-29281-0, 1995*. 1995. **99**(5): p. 787-787.
73. Perkampus, H.-H., *UV-VIS Spectroscopy and its Applications*. 2013: Springer Science & Business Media.
74. Clark, B., T. Frost, and M. Russell, *UV Spectroscopy: Techniques, instrumentation and data handling*. Vol. 4. 1993: Springer Science & Business Media.
75. *http://www.buzzle.com/articles/lcr-meter-working-principle-anduses.html*.
76. *https://www.electronics-notes.com/articles/test-methods/lcr-meter-bridge/primer-basics.php.*
77. Nagaraju, G., et al., *Electrochemical heavy metal detection, photocatalytic, photoluminescence, biodiesel production and antibacterial activities of Ag–ZnO nanomaterial.* 2017. **94**: p. 54-63.
78. Khabbaz, M., M.H.J.J.o.c. Entezari, and i. science, *Simple and versatile one-step synthesis of FeS2 nanoparticles by ultrasonic irradiation.* 2016. **470**: p. 204-210.
79. Kahn, M.L. and Z.J.J.A.P.L. Zhang, *Synthesis and magnetic properties of CoFe 2 O 4 spinel ferrite nanoparticles doped with lanthanide ions.* 2001. **78**(23): p. 3651-3653.